

TKK Dissertations 101  
Espoo 2008

**CHARACTERIZATION OF TRANSPORT PHENOMENA IN  
SMALL POLYMER ELECTROLYTE MEMBRANE FUEL  
CELLS**

Doctoral Dissertation

**Olli Himanen**



**Helsinki University of Technology  
Faculty of Information and Natural Sciences  
Department of Engineering Physics**

TKK Dissertations 101  
Espoo 2008

# **CHARACTERIZATION OF TRANSPORT PHENOMENA IN SMALL POLYMER ELECTROLYTE MEMBRANE FUEL CELLS**

Doctoral Dissertation

**Olli Himanen**

Dissertation for the degree of Doctor of Science in Technology to be presented with due permission of the Faculty of Information and Natural Sciences for public examination and debate in Auditorium K216 at Helsinki University of Technology (Espoo, Finland) on the 1st of February, 2008, at 12 noon.

**Helsinki University of Technology  
Faculty of Information and Natural Sciences  
Department of Engineering Physics**

**Teknillinen korkeakoulu  
Informaatio- ja luonnontieteiden tiedekunta  
Teknillisen fysiikan laitos**

Distribution:

Helsinki University of Technology  
Faculty of Information and Natural Sciences  
Department of Engineering Physics  
P.O. Box 4100  
FI - 02015 TKK  
FINLAND  
URL: <http://www.tkk.fi/Units/AES/>  
Tel. +358-9-451 3198  
Fax +358-9-451 3195  
E-mail: [olli.himanen@tkk.fi](mailto:olli.himanen@tkk.fi)

© 2008 Olli Himanen

ISBN 978-951-22-9146-5  
ISBN 978-951-22-9147-2 (PDF)  
ISSN 1795-2239  
ISSN 1795-4584 (PDF)  
URL: <http://lib.tkk.fi/Diss/2008/isbn9789512291472/>

TKK-DISS-2413

Multiprint Oy  
Espoo 2008



ABSTRACT OF DOCTORAL DISSERTATION		HELSINKI UNIVERSITY OF TECHNOLOGY P.O. BOX 1000, FI-02015 TKK <a href="http://www.tkk.fi">http://www.tkk.fi</a>	
Author Olli Pekka Himanen			
Name of the dissertation Characterization of transport phenomena in small polymer electrolyte membrane fuel cells			
Manuscript submitted 12.6.2007		Manuscript revised 13.11.2007	
Date of the defence 1.2.2008			
<input type="checkbox"/> Monograph		<input checked="" type="checkbox"/> Article dissertation (summary + original articles)	
Department	Engineering Physics		
Laboratory	Advanced energy systems		
Field of research	fuel cells		
Opponent(s)	Ph.D. Preben Vie		
Supervisor	Prof. Peter Lund		
Instructor	D.Sc. Tero Hottinen		
<b>Abstract</b> In small fuel cell systems, energy consumption and size of auxiliary devices should be minimized. One option is to use passive controlling methods that rely on material and structural solutions. Therefore it is important to understand transport phenomena occurring in the cells. In this thesis, charge, mass, and heat transport phenomena related to small PEMFCs were studied experimentally and by modeling.  A new method was developed for the characterization of water transport properties of polymer electrolyte membrane under realistic operating conditions. The method was used to evaluate the diffusion coefficient of water in the membrane.  Due to channel-rib structure, cell components are inhomogeneously compressed. Charge and mass transport parameters were experimentally evaluated as a function of compression. The effect of inhomogeneous compression on cell operation was studied by modeling. Inhomogeneous compression does not significantly affect the polarization behavior of the cell, but it creates uneven current and temperature distributions inside the cell. This affects both cell performance and life-time and should not be ignored in cell design and modeling.  The operation of a free-breathing PEMFC was studied at subzero temperatures. To be able to operate at low temperatures, current density must be high enough to avoid freezing of reactant product water inside the cell. Start-up at cold temperatures requires active heating.  To maximize fuel efficiency, the operation of a free-breathing PEMFC in dead end mode was investigated. Dead ended operation with periodic purging enables high fuel utilization rate and the test cell operated without significant water management problems or performance loss.			
Keywords PEMFC, transport phenomena, membrane, water management, free-breathing			
ISBN (printed)	978-951-22-9146-5	ISSN (printed)	1795-2239
ISBN (pdf)	978-951-22-9147-2	ISSN (pdf)	1795-4584
Language	english	Number of pages	60 + app. 65
Publisher	Department of Engineering Physics		
Print distribution	Laboratory of Advanced Energy Systems		
<input checked="" type="checkbox"/> The dissertation can be read at <a href="http://lib.tkk.fi/Diss/2008/isbn9789512291472/">http://lib.tkk.fi/Diss/2008/isbn9789512291472/</a>			





VÄITÖSKIRJAN TIIVISTELMÄ	TEKNILLINEN KORKEAKOULU PL 1000, 02015 TTK <a href="http://www.tkk.fi">http://www.tkk.fi</a>
Tekijä Olli Pekka Himanen	
Väitöskirjan nimi Pienten polymeeripolttokennojen kuljetusilmiöiden karakterisointi	
Käsikirjoituksen päivämäärä 12.6.2007	Korjatun käsikirjoituksen päivämäärä 13.11.2007
Väitöstilaisuuden ajankohta 1.2.2008	
<input type="checkbox"/> Monografia	<input checked="" type="checkbox"/> Yhdistelmäväitöskirja (yhteenvedo + erillisartikkelit)
Osasto	Teknillinen fysiikka
Laboratorio	Energiatieteet
Tutkimusala	Polttokennot
Vastaväittäjä(t)	Ph.D. Preben Vie
Työn valvoja	Professori Peter Lund
Työn ohjaaja	TkT Tero Hottinen
<b>Tiivistelmä</b> <p>Pienissä polttokennojärjestelmissä on tärkeää minimoida oheisjärjestelmien koko ja energiankulutus, jonka vuoksi kennon ohjauksessa pyritään käyttämään passiivisia järjestelmiä. Passiivinen ohjaus perustuu materiaali- ja rakenneratkaisuihin, joten suunnittelu- ja kehitystyön kannalta kennossa tapahtuvien kuljetusilmiöiden tunteminen on tärkeää. Tässä työssä tutkittiin polymeeripolttokennossa tapahtuvia aineen-, varauksen- ja lämmönsiirtoilmiöitä kokeellisesti ja mallintamalla.</p> <p>Elektrolyyttinä käytettävän polymeerimembraanin vedenkuljetusominaisuuksien tutkimiseen kehitettiin uusi menetelmä, jonka tuloksena ominaisuudet pystytään määrittämään todellisissa toimintaolosuhteissa. Menetelmällä määritettiin veden diffuusiokerroin polymeerimembraanissa.</p> <p>Polymeeripolttokennon virtauskanaviston rakenne aiheuttaa kennon komponentteihin epätasaisen puristuksen. Aineen- ja varauksensiirtoa kuvaavien parametrien riippuvuus puristuksesta määritettiin kokeellisesti ja ilmiön vaikutukset kennon toimintaan selvitettiin mallintamalla. Epätasainen puristuma ei vaikuta merkittävästi kennon polarisaatiokäyttäytymiseen, mutta aiheuttaa epätasaiset virta- ja lämpötilajakaumat kennon sisälle. Ilmiöllä on tärkeä merkitys kennon suorituskyvyn ja eliniän kannalta ja se täytyy huomioida kennosuunnittelussa ja mallintamisessa.</p> <p>Vapaastihengittävän polymeeripolttokennon toimintaa tutkittiin kylmissä olosuhteissa. Kennon toiminta kylmässä edellyttää riittävän suurta virrantiheyttä ja lämmöntuottoa estämään veden jäätyminen kennon sisällä. Kylmäkäynnistys edellyttää matalassa lämpötilassa erillistä kuumennusjärjestelmää.</p> <p>Vapaastihengittävän kennon toimintaa testattiin korkealla polttoaineen käyttöasteella hyötysuhteen maksimoimiseksi. Kenno toimi korkeilla polttoaineen käyttöasteilla ilman merkittäviä vedenhallintaongelmia tai suorituskyvyn alenemista.</p>	
Asiasanat polymeeripolttokenno, kuljetusilmiöt, membraani, vedenhallinta, vapaastihengittävä	
ISBN (painettu) 978-951-22-9146-5	ISSN (painettu) 1795-2239
ISBN (pdf) 978-951-22-9147-2	ISSN (pdf) 1795-4584
Kieli Englanti	Sivumäärä 60 + liit. 65
Julkaisija Teknillisen fysiikan osasto	
Painetun väitöskirjan jakelu Energiatieteet-laboratorio	
<input checked="" type="checkbox"/> Luettavissa verkossa osoitteessa <a href="http://lib.tkk.fi/Diss/2008/isbn9789512291472/">http://lib.tkk.fi/Diss/2008/isbn9789512291472/</a>	



# Table of Contents

Abstract .....	3
Tiivistelmä .....	5
Preface .....	9
List of publications .....	11
<b>1. Introduction .....</b>	<b>13</b>
<b>2. PEMFC Technology.....</b>	<b>15</b>
2.1. General .....	15
2.2. Fuel Cell Components .....	16
2.2.1. Membrane Electrode Assembly.....	16
2.2.2. Porous Transport Layers .....	16
2.2.3. Flow Field Plates .....	17
2.2.4. Other Components.....	17
2.3. Free-Breathing PEMFC.....	18
2.4. Cell Performance .....	19
2.4.1. Open-Circuit Voltage .....	19
2.4.2. Current-Voltage Behavior.....	19
2.4.3. Potential Profile .....	21
2.5. Water Management.....	22
<b>3. Characterization of MEA .....</b>	<b>25</b>
3.1. Background .....	25
3.2. Methods.....	25
3.2.1. Experimental.....	25
3.2.2. Modeling .....	28
3.3. Results .....	30
<b>4. Water Management of a Free-Breathing PEMFC under Various Operating Conditions.....</b>	<b>34</b>
4.1. Background .....	34
4.2. Methods.....	34
4.2.1. Sub-Zero Tests.....	34
4.2.2. Dead-End Tests.....	35
4.3. Results .....	36
4.3.1. Sub-Zero Tests.....	36
4.3.2. Dead-End Experiments .....	39
<b>5. Inhomogeneous Compression of Porous Transport Layer .....</b>	<b>42</b>
5.1. Background .....	42
5.2. Experimental .....	43
5.2.1. PTL Intrusion into Channel .....	43
5.2.2. Gas Permeability .....	43
5.2.3. Electrical Conductivity and Contact Resistance.....	44
5.3. Modeling .....	46
5.4. Results .....	47
5.4.1. Experimental.....	47
5.4.2. Modeling .....	49
<b>6. Summary and Conclusions.....</b>	<b>53</b>
References.....	55



## Preface

The work presented in this thesis has been carried out in the Laboratory of Advanced Energy Systems at Helsinki University of Technology between 2003 and 2007. This work was mainly funded by the Academy of Finland. Other supporters are Finnish Funding Agency of Technology and Innovation (TEKES), The Graduate School for Energy Science and Technology (Energiatekniikan Tutkijakoulu), and Foundation of Technology Promotion (Tekniikan Edistämissäätiö).

I would like to thank my supervisor Peter Lund for giving me the opportunity and freedom to work with this interesting and challenging topic. My instructor Tero Hottinen is also gratefully acknowledged, it has been very rewarding to work with you. This work is a result of a fruitful collaboration done together with the former and current members of the fuel cell group, Tuomas Mennola, Matti Noponen, Mikko Mikkola, Suvi Karvonen, Iwao Nitta, Jaakko Saarinen, Timo Lehtinen, Kim Åström, Sonja Jokimies, Saara Tuurala, I thank you all. Great thanks also for other colleagues for creating a pleasant and productive atmosphere. I would like to thank Ville Saarinen from the Department of Chemistry for the very rewarding collaboration. Jari Ihonen, and Michael Vunnucky, who acted as pre-examinators, gave very important critical comments and suggestions about the manuscript, thank you very much for that.

Suuret kiitokset vanhemmilleni Pirjolle ja Laurille sekä veljelleni Tuomakselle kaikesta antamastanne tuesta.

Lopuksi haluan sanoa kiitokset Rakkaalleni, Jatalle. Sun kanssa on hyvä elää.

Espoo, January 2008



## List of publications

This thesis is an article dissertation and includes the following publications:

- I Olli Himanen, Tero Hottinen, Mikko Mikkola, Ville Saarinen, “*Characterization of membrane electrode assembly with hydrogen-hydrogen cell and ac-impedance spectroscopy Part I. Experimental*”, *Electrochimica Acta* 52, pp. 206-214, 2006
- II Olli Himanen, Tero Hottinen, “*Characterization of membrane electrode assembly with hydrogen-hydrogen cell and ac-impedance spectroscopy Part II. Modeling*”, *Electrochimica Acta* 52, pp. 581-588, 2006
- III Olli Himanen, Tero Hottinen, Saara Tuurala, “*Operation of a planar free-breathing PEMFC in a dead-end mode*”, *Electrochemistry Communications* 9, pp. 891-894, 2007
- IV Tero Hottinen, Olli Himanen, Peter Lund, “*Performance of planar free-breathing PEMFC at temperatures below freezing*”, *Journal of Power Sources* 154, pp. 86-94, 2006
- V Iwao Nitta, Tero Hottinen, Olli Himanen, Mikko Mikkola, “*Inhomogeneous compression of PEMFC gas diffusion layer Part I. Experimental*”, *Journal of Power Sources* 171, pp. 26-36, 2007
- VI Tero Hottinen, Olli Himanen, Suvi Karvonen, Iwao Nitta, “*Inhomogeneous compression of PEMFC gas diffusion layer Part II. Modeling the effect*”, *Journal of Power Sources* 171, pp. 113-121, 2007
- VII Tero Hottinen, Olli Himanen, “*PEMFC temperature distribution caused by inhomogeneous compression of GDL*”, *Electrochemistry Communications* 9, pp. 1047-1052, 2007

For Publications I, II, and III, the author was mainly responsible for all parts of the publications.

For Publication IV, the author was responsible for the design and construction of measurement system, and participated actively in the design and conduction of experiments. The author participated in the analysis of measurement results and in the writing process.

For Publication V, the author participated actively in the design of experimental devices and experiments, and in the analysis of measurement results. The author also participated in the writing process.

For Publication VI, the author assisted in the build-up of the model and in the writing process.

For Publication VII, the author participated in the writing process.



# 1. Introduction

Fossil fuels are the main primary energy source in the world today. Due to environmental and political reasons, economically and ecologically viable energy sources and conversion techniques are needed in the future. Fuel cells enable conversion of fuel into electricity and heat with high efficiency and low emissions. If hydrogen is used as the fuel, the only reaction product is water. However, hydrogen does not exist in free form on the Earth and must be produced using other primary energy sources. Combined with suitable hydrogen production and distribution methods, fuel cells offer a carbon free energy chain.

Fuel cell is an old invention, first published by Prof. Schönbein in 1839. First prototype fuel cells were introduced by Sir William Grove in 1842. Fuel cells were used to produce electricity on the first space missions and fuel cell development took giant leaps in 1950s and 1960s. Polymer electrolyte membrane fuel cell (PEMFC), for example, was developed for the Gemini missions. Currently, the most important drivers and application areas for fuel cell development are the automotive industry, portable electronic devices, and distributed energy production.

The electrolyte material used in PEMFCs needs water to maintain proton conductivity, but excess water hinders reactant transfer inside the cell. Because of these two opposite needs, water management is one of the most important issues related to PEMFC systems and has a significant effect on life-time and performance. Water management can be done actively in large systems using humidifiers, heaters, and air pumps. In small PEMFC systems, e.g. in portable electronics, these external devices are not desirable due to their power consumption and size, and therefore passive methods are more suitable. Passive operation and water management are based on material and structural solutions and therefore understanding of transport phenomena and material parameters is essential. The goal of this thesis was to increase understanding of transport phenomena in small PEMFCs, which is important for their development.

Membrane electrode assembly (MEA) is the heart of PEMFC and the knowledge of water transport properties of the MEA is important for the successful water management of the cell. A new method was developed for the characterization of water and charge transport properties of MEA under realistic operating conditions. The method was used to evaluate the diffusion coefficient of water in the membrane and membrane conductivity. The method is useful for the development of new MEAs and for the choice of suitable MEA for each application.

Channel-rib structure of flow field plate creates inhomogeneous compression pressure inside the PEMFC, which affects especially the properties of porous transport layers (PTLs). Charge and mass transfer properties of PTLs were experimentally evaluated as a function of compression. A computer model was developed to see the effects of inhomogeneous compression on the PEMFC performance. Inhomogeneous compression does not significantly affect the polarization behavior of the cell, but it creates uneven current and temperature distributions inside the cell, which decrease cell performance and lifetime. Inhomogeneous compression should be taken into account in PEMFC design and modeling.

Power sources of portable electronic devices must operate under different ambient conditions and provide high energy density. Therefore, water management of a small PEMFC was investigated under different operating conditions, at subzero temperatures and also with high fuel utilization rates. It was found that the cell is able to operate at very cold temperatures if current density and heat production are high enough to avoid freezing of water inside the cell. For start-up at cold temperatures, the cell needs active heating. With high fuel utilization rates, the cell operated without significant performance loss or water management problems. These results support the feasibility of free-breathing PEMFCs and are important for their further development and commercialization.

This thesis starts with a short description of the PEMFC, cell components and water management in Chapter 2. Chapters 3-5 summarize Publications I-VII that deal with different PEMFC related transport phenomena. Summary and conclusions of this work, as well as suggestions for further research are given in Chapter 6.

## 2. PEMFC Technology

### 2.1. General

In this chapter the structure and components of PEMFC are introduced as well as performance and water management issues. Also corresponding links to the publications of the thesis are indicated.

PEMFC is an electrochemical device that converts the chemical energy of reactants directly into electricity and heat. Hydrogen is used as fuel and it is oxidized into protons at the anode. Protons are transported to cathode through the proton conducting polymer electrolyte membrane and electrons through an external load. Protons and electrons react with oxygen at the cathode producing water. Schematic structure of PEMFC and cell reactions are illustrated in Figure 1.

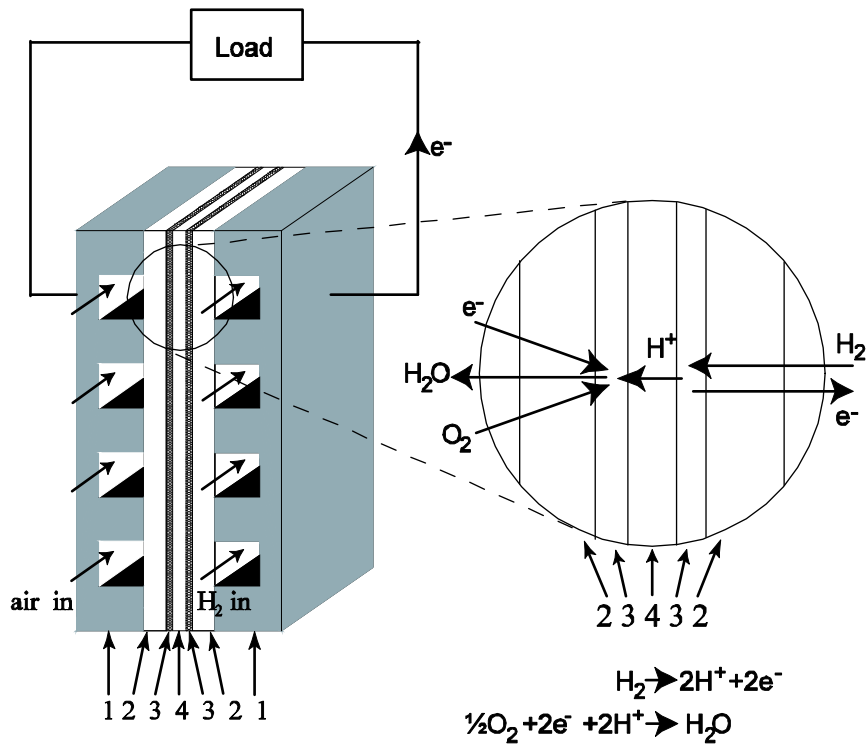


Figure 1. Schematic of PEMFC. Numbers refer to following components 1: flow field plates, 2: porous transport layers, 3: electrodes, 4: membrane

PEMFCs produce electricity with high efficiency, up to 60 % (LHV) [1], with very low emissions at the time of use. Therefore, most of the car manufacturers are actively developing PEMFC technology to replace the internal combustion engines as vehicle power source. In the smaller power range, functionality and power consumption of portable electronic devices is increasing and the current battery technologies can not keep up with the increasing demand. PEMFC combined with a suitable fuel storage would provide longer operating times and therefore electronics manufacturers are developing small fuel cell systems.

## **2.2. Fuel Cell Components**

### **2.2.1. Membrane Electrode Assembly**

The most important component of a PEMFC is the MEA. An MEA consists of a proton conducting electrolyte membrane which is located between thin film electrodes. Electrodes used in PEMFC are approximately 10  $\mu\text{m}$  thick porous structures that contain platinum catalyst. Thin film electrodes with low platinum loading were developed in the early 1990s [2] and are one of the most important development steps for PEMFCs. Electrochemical reactions take place at a so called three-phase boundary, where electron conductor, proton conductor and reactants meet. To enhance the reaction rate, this three-phase boundary must occur on the surface of the catalyst particle. To achieve this, electrodes are usually made of a mixture of electrically conducting carbon black, proton conducting ionomer, carbon supported platinum catalyst, and solvent. During the manufacturing process, solvent is evaporated, which creates the porous structure. Typical platinum loading of thin film electrodes is from 0.1 to 0.4  $\text{mg cm}^{-2}$ . At the operating temperatures of PEMFC, platinum catalyst is sensitive to fuel impurities, especially to carbon monoxide. Non-noble and platinum-alloy catalyst materials are investigated to reduce price, achieve better tolerance for impurities and enhance durability of catalyst, see e.g. [3, 4].

The membrane is a solid electrolyte film that conducts protons from anode to cathode. The membrane has to be electronic insulator, good proton conductor, mechanically and chemically durable and impermeable to gases. The most common electrolyte material used today is Nafion<sup>®</sup> developed by E.I. du Pont de Nemours and Company. Nafion<sup>®</sup> is a sulfonated tetrafluoroethylene copolymer and it is used in PEMFCs in its  $\text{H}^+$ -form. Other electrolyte materials are e.g. Flemion<sup>®</sup> (Asahi Glass Co.) and reinforced composite Gore-Select<sup>®</sup> (W.L. Gore & Associates) [5]. The proton conducting mechanisms in these polymers are assumed to be the vehicle and Grotthuss mechanisms, see e.g. [6, 7]. In vehicular mechanism, hydrated proton (e.g.  $\text{H}_3\text{O}^+$ ) moves through an aqueous environment, similarly to normal molecular diffusion. In Grotthuss mechanism, also called Grotthuss hopping, proton moves along a chain of hydrogen bonded water molecules. These transport mechanisms need water for proton transport and therefore proton conductivity of these polymers is strongly dependent on the water content, see e.g. [8-10]. A new method for the characterization of MEA is presented in Publications I and II.

### **2.2.2. Porous Transport Layers**

PTLs are located between the electrodes and flow field plates. PTLs are also known as porous backings, gas diffusion layers (GDLs) or gas diffusion backings (GDBs). They create a pathway for reactants from the flow channels to the electrode surface. Also reaction product water and water from humidified reactants passes through the PTLs. In addition, PTL conducts electrons and heat between the electrode and flow field plate and gives mechanical support to the MEA. Most commonly used PTL materials are porous carbon papers and cloths. Usually some substance, for example PTFE is used to increase hydrophobicity of PTL and to achieve better water management properties. It is assumed that liquid water is transported through hydrophilic pores, whereas gas-phase transport occurs through hydrophobic pores of PTL, see e.g. [11, 12]. Microporous

layers (MPL) made of carbon black and hydrophobic substance are usually added onto the PTL surface to improve the cell performance, see e.g. [12].

Due to the channel-rib structure of the flow field plate, PTL is compressed unevenly. PTL is compressed under the ribs, but remains almost uncompressed under the channels. Compression increases the electrical and thermal conductivity of the PTL, and decreases electrical and thermal contact resistances between components. Gas permeability and porosity are also changed by compression. The effects of inhomogeneous compression of PTL on the transport phenomena and performance of PEMFC were studied in Publications V, VI, and VII.

### **2.2.3. Flow Field Plates**

Flow field plates distribute reactants to PTLs and remove excess water from the cell. They also conduct electrons and heat and support PTLs mechanically. Flow field plates are usually made of graphite, steel, graphite composite or some other conducting and chemically stable material. The most commonly used channel geometries are the serpentine channel, parallel channels and their combinations. Interdigitated channels and net structures are also used. Different channel structures have been studied in e.g. [13-15].

To achieve a higher output voltage, single cells are normally connected electrically into series, i.e. they form a fuel cell stack. This is done with so called bipolar plates, which are two-sided flow-field plates, and they provide oxygen and hydrogen for neighboring cells. Coolant circulation channels or cooling ribs are usually integrated into bipolar plates to remove excess heat produced in the cell.

### **2.2.4. Other Components**

A fuel cell also needs gaskets and end-plates for gas tightness and mechanical rigidity. Gaskets are made of chemically inert gas impermeable material, e.g. some rubbers and PTFE impregnated glass fiber are suitable. End-plates and some tightening mechanism such as bolts and nuts are used to compress components of the cell together. They also provide mechanical support for other components to minimize their bending and to equalize the contact pressure on the active area of the cell, see e.g. [16, 17]. A fuel cell has to be connected electrically to an external load and it is usually done with current collectors. Current collectors are made of a highly conductive material and they are connected to the outermost flow field plates.

A fuel cell system needs also auxiliary components to optimize system performance and life-time. These include air pumps and fans, mass flow controllers, gas humidifiers and purifiers, a temperature controlling system etc. These auxiliary components increase the system complexity and power consumption, and therefore especially in small-scale applications passive controlling and operating methods are used. Due to passive operation, so called free-breathing PEMFC is a potential power source for small-scale applications.

### 2.3. Free-Breathing PEMFC

This thesis focuses on characterization of transport phenomena of small-scale PEMFCs. In portable electronic devices and other small-scale fuel cell applications, the energy density of the power source must be as high as possible. One way to maximize energy density is to minimize the energy consumption of auxiliary devices. Free-breathing cells are one option, because they take the oxygen passively from the surrounding air and power consuming air pumps or blowers are not needed. However, passive operation and control methods make the water management challenging.

A free-breathing PEMFC with vertical straight cathode channels has been studied by current distribution measurements and modeling [18-21]. It was concluded that the cathode side mass transport is the most important performance limiting factor in that cell type. Passive oxygen transport was not sufficient and the cell was prone to flooding. Therefore a free-breathing cell with open cathode structure was developed [22, 23]. In this cell type there are no cathode side air channels at all and the cathode side PTL is in direct contact with ambient air through openings in the cathode current collector/end plate. The structure of this cell type is shown in Figure 2. This structure improves mass transport at cathode side. Especially excess water removal is enhanced, which decreases flooding of the cell and makes the water management easier.

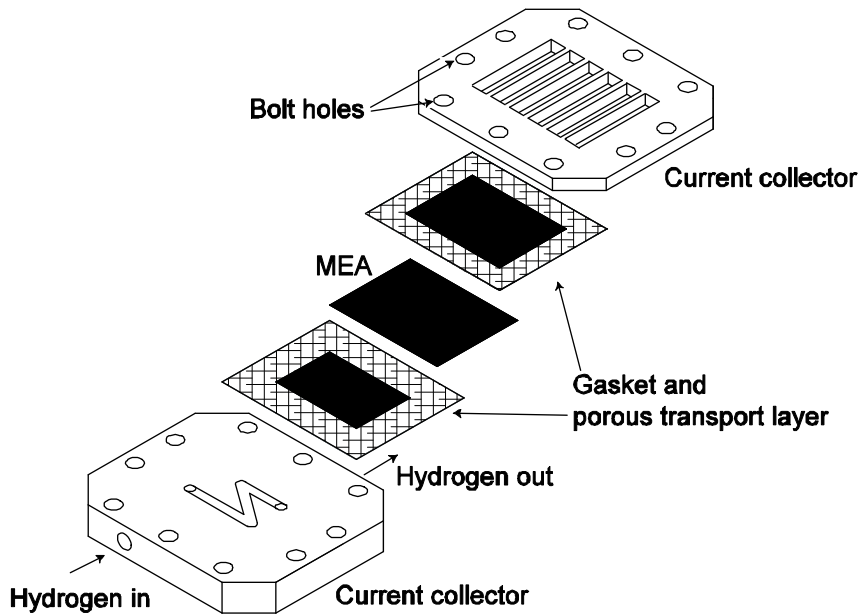


Figure 2. Structure of a free-breathing PEMFC. Modified from [22].

Free-breathing PEMFCs without cathode side channels have been developed and studied extensively by various research groups. Jeong et al. [24] studied the effects of cathode open area and ambient humidity on the performance of free-breathing PEMFC and they achieved a maximum power density of  $146 \text{ mW cm}^{-2}$ . Schmitz et al. [25, 26] developed a planar free-breathing PEMFC based on printed circuit board technology. They minimized the thickness of the cell to 3.5 mm and tested different PTLs and cathode structures and achieved a  $100 \text{ mW cm}^{-2}$  power density. Hahn et al. [27] developed a  $80 \mu\text{m}$  thick cell with an  $80 \text{ mW cm}^{-2}$  stable power density. Tabe et al. [28]

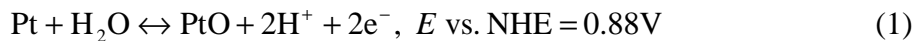
tested different cathode structures and concluded that the traditional channel type flow-field plate is superior to open cathode structure due to smaller contact resistances. With an open cathode structure they achieved an  $80 \text{ mWcm}^{-2}$  power density and with a channel-type cathode  $105 \text{ mWcm}^{-2}$ . The measured maximum stable power density of the free-breathing PEMFC used in Publications III and IV is  $260 \text{ mW cm}^{-2}$ , and maximum peak power density is  $500 \text{ mW cm}^{-2}$  [23, 29].

Free-breathing PEMFCs are in close contact with ambient air and in real applications they have to operate under different ambient conditions with high efficiency. Different ambient conditions and passive control methods make water management of these small cells very challenging. Therefore it is important to have knowledge about transport phenomena occurring inside the cells. Transport phenomena inside the MEA were studied in Publications I and II. Publications V, VI, and VII focus on the transport phenomena inside the PTLs. In Publications III and IV, it was studied how water management of a free-breathing PEMFC can be arranged when the cell is operated with high fuel utilization rate or at low temperatures.

## **2.4. Cell Performance**

### **2.4.1. Open-Circuit Voltage**

A theoretical reversible voltage of a PEMFC at  $25 \text{ }^\circ\text{C}$  and 1 bar is 1.23 V, when the reaction product water is in liquid form and pure oxygen is used as the oxidant. Real open-circuit voltage, OCV, is significantly lower, typically 0.9-1.1 V depending on the operating conditions and cell materials. This significant voltage decrease is assumed to be caused mainly by mixed potentials, see e.g. [30]. A mixed potential is formed as a combination of different reactions occurring at the cathode, one is normal water formation, but another one is oxidation of platinum:



This parallel reaction decreases OCV by almost 0.2 V at room temperature [30].

Hydrogen that has permeated to the cathode oxidizes and causes mixed potentials, but also reduces the oxygen surface concentration. The effect of this hydrogen crossover on the OCV decrease has been calculated to be approximately 50 mV with Nafion 112 at room temperature [30].

### **2.4.2. Current-Voltage Behavior**

When current is drawn from the cell, voltage decreases from the OCV due to activation, resistive and mass transfer losses. These losses are also usually called as overpotentials. Their effect can be seen in a typical current-voltage curve of a PEMFC illustrated in Figure 3.

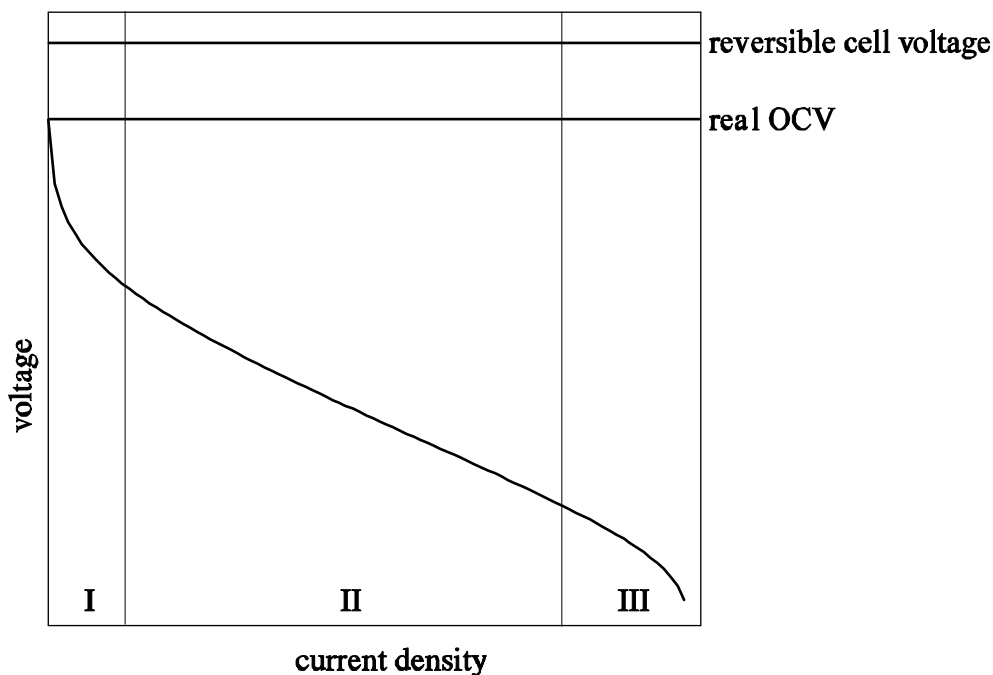


Figure 3. Polarization curve of a PEMFC. I:activation overpotential, II:resistive overpotential, and III:mass transfer overpotential defines the shape of the curve.

At low current densities (region I), voltage decreases logarithmically as a function of current density due to activation losses. Activation losses are mainly caused by the activation energy needed to drive the cathode reaction. Activation losses of the anode reaction are much smaller due to faster reaction kinetics. Activation overpotential and decreased OCV typically form the largest portion of PEMFC voltage losses. Reaction kinetics of the anode reaction were studied in Publications I and II.

In the middle part of polarization curve (region II), voltage decreases rather linearly, mainly due to resistive losses both in electron and ion conductors. Resistive losses occur in every fuel cell component and at the interfaces between them. The main source of resistive losses is usually the ionic resistance of the membrane. The conductivity of membrane was studied in Publication I and II. Bulk conductivity and contact resistance of PTL were studied in Publications V, VI, and VII.

At high current density (region III), cell voltage starts to decrease rapidly due to mass transfer limitations. Sluggish reactant transport to electrode surfaces and removal of reaction product water decrease concentrations of reactants at three-phase boundaries. This leads into rapid decrease in cell voltage. Mass transport is one of the key issues of this thesis and mass transport in different cell components was studied in Publications I-VII.

Activation and mass transfer overpotentials can be represented by the current-overpotential Equation (2), see e.g. [31]

$$i = i_0 \left[ \frac{c_O}{c_O^*} \exp\left(-\frac{\alpha z F}{RT} \eta\right) - \frac{c_R}{c_R^*} \exp\left(\frac{(1-\alpha) z F}{RT} \eta\right) \right], \quad (2)$$

where  $i$  is the current density,  $i_0$  is the exchange current density,  $c_O^*$  and  $c_R^*$  are reference concentrations of oxidant and reductant,  $c_O$  and  $c_R$  are their concentrations at the reaction site,  $\alpha$  is the charge transfer coefficient,  $z$  is the number of electrons transferred,  $F$  is the Faraday constant,  $R$  is the molar gas constant,  $T$  is temperature, and  $\eta$  is the overpotential. In the case of a PEMFC cathode, eigenvalue of overpotential is large and Equation (2) can be approximated by, see eg. [32, 33].

$$i = i_0 \frac{c_O}{c_O^*} \exp\left(-\frac{\alpha z F}{RT} \eta\right). \quad (3)$$

Overpotential is defined with Equation (4)

$$\eta = E - E_0, \quad (4)$$

where  $E$  is the potential difference between two phases (ion-conductor and electron conductor) in current state and  $E_0$  is their potential difference in equilibrium state.

Mass transport losses are connected to the cell voltage by Equations (2) and (3). Sluggish mass transport decreases  $c_O$  (in this case, concentration of oxygen), which decreases cell voltage.

### 2.4.3. Potential Profile

There are different charge carriers in a PEMFC, i.e. electrons and protons, which have their own potential levels. A schematic PEMFC potential profile is presented in Figure 4. The potential of anode side flow field plate/current collector is usually fixed to 0 V and the cell voltage is the potential difference between anode and cathode flow field/current collector plates. Stepwise potential drops between cell components are due to contact resistances.

Overpotential of the anode,  $\eta_a$ , is the potential difference between electron and proton conductor

$$\eta_a = \Phi_M - \Phi_S, \quad (5)$$

where  $\Phi_M$  is the potential of proton conductor, and  $\Phi_S$  is the potential of electron conductor. Equilibrium voltage of anode reaction is zero.

Cathode overpotential is

$$\eta_c = \Phi_S - \Phi_M - E_0. \quad (6)$$

For pure cathode reaction,  $E_0$  would be 1.23 V. Due to the above mentioned mixed potentials, the real OCV is typically used in PEMFC modeling as  $E_0$  to get similar polarization behavior as in experiments.

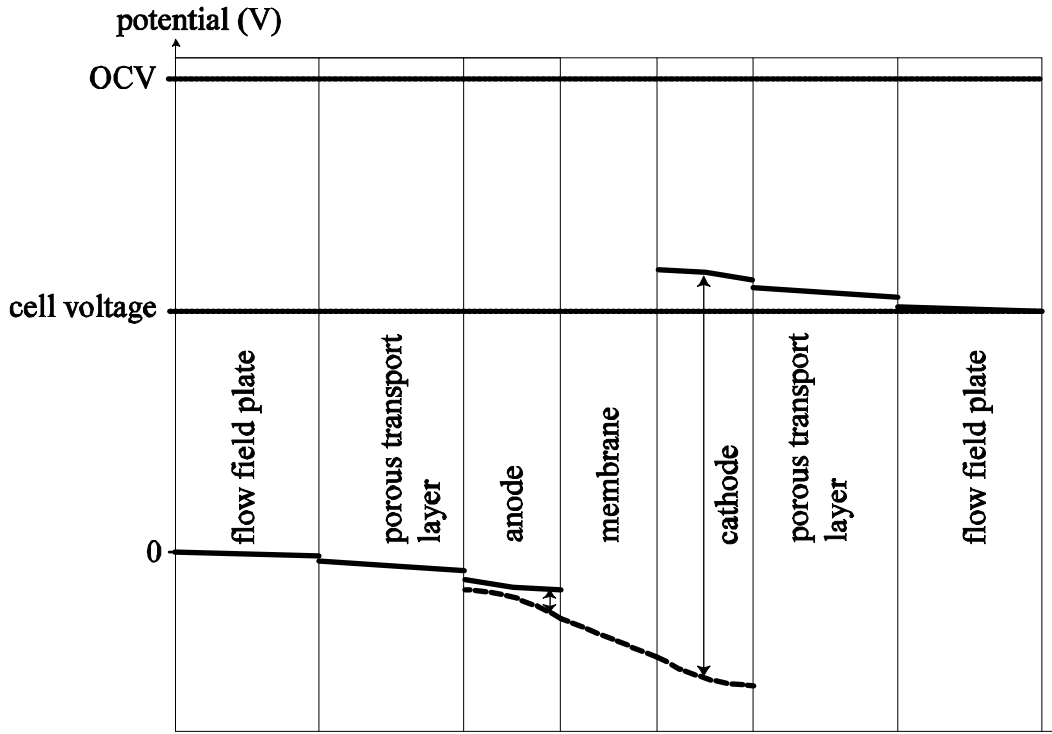


Figure 4. Potential profile through a PEMFC. Solid line: potential of electron conductor, dashed line: potential of proton conductor. Arrows indicate the potential difference between different phases. Stepwise potential drops between cell components are due to contact resistances.

## 2.5. Water Management

Proton conductivity of sulphonated ionomer materials depends on their water content. Higher the water content, higher the conductivity. Conductivity is the highest when the ionomer is in contact with liquid water, see e.g. [34, Publication I]. On the other hand, liquid water hinders mass transport in the electrodes, porous transport layers and gas channels, which decreases cell performance. Because of these two opposite needs, water management is an essential issue to obtain good and reliable performance. The objective of water management is to minimize losses caused by ionomer resistance and mass transport and to maximize the life-time of the cell.

Water management can be done actively by controlling the operating parameters, such as flow rate and humidity of inlet gases, and temperature of the cell. Due to increased complexity and system size, most of the active controlling methods are not suitable for small portable applications. In such applications, passive controlling methods should be used where possible. Passive water management methods include material and

structural choices, and properties of porous transport layer and flow field geometry have a significant effect on water management and cell performance [1, 35- 40].

Water is produced at the cathode, and some part of it is transferred through the membrane to the anode side of the cell. Water is removed from the cell with exiting reactant flows. Water is transported in the membrane by three mechanisms: diffusion, electro-osmotic drag, and hydraulic permeation. Diffusion is caused by the water concentration gradient and it is usually described by the Fick diffusion [41- 44] or multicomponent diffusion [45- 47]. Proton flux causes the electro-osmotic drag and depending on the membrane water content, the number of water molecules dragged by one proton varies from 1 to 6 [34, 48-50]. Hydraulic permeation is caused by the pressure gradient over the membrane. Pressure gradient drives water from high pressure side to low pressure side. Water transport by hydraulic permeation has been studied in e.g. [50, 51]. The diffusive water transport in membrane was studied in Publications I and II.

The main methods to evaluate diffusion coefficient of water in the polymer membrane are total water flux measurements [52-55] and NMR spectroscopy [10, 56, 57]. A few studies have been published based on water uptake or desorption dynamics [58, 59], or radiotracer measurements [60, 61].

In the total water flux method, the amount of water going in to the cell on one or both sides is controlled and the amount of water coming out from the cell is measured. The total water flux going through the membrane can be calculated from the difference between in-going and out-coming humidities. The main problem in this method are the spatial variations in the humidity levels inside the cell, and therefore analysis of measurement results with modeling is an important part of this technique as shown in Publications I and II. Spatial variations in the humidity level could be minimized by increasing gas flow rates and decreasing the area of the membrane. However, more accurate humidity measurements would be needed.

In NMR spectroscopy, the intradiffusion coefficient of  $H^+$  is measured with pulsed-gradient magnetic field and it is then identified to be similar with  $H_2O$  [10]. This intradiffusion coefficient can be converted into normal Fickian diffusion coefficient by multiplying it by  $\frac{\partial \ln a}{\partial \ln c}$ , where  $a$  is the activity and  $c$  is the concentration of diffusing species [10].

The goal of water management is to maximize the cell performance and life-time and one important parameter affecting the performance is the conductivity of the membrane. Due to the charge carrier, the proton conductivity of polymer membrane can not be measured directly with a normal ohmmeter. Suitable methods are the current interruption method, e.g. [62-64], and AC-impedance spectroscopy, e.g. [37, 38, 65-67]. In the current interruption method, cell current is stepwise changed and voltage transient is recorded. The time constant of ohmic losses is significantly smaller than that of activation or mass transfer losses and rapid change in the cell voltage is mainly caused by ohmic losses. Unfortunately, this rapid voltage change is interfered by three factors,

the ringing of the signal due to parasitic resonances, imperfect characteristics of the electronic switch, and also relaxation of other overpotentials [68]. Transient analysis can be done in frequency domain, using the same tools as in AC-impedance spectroscopy described below [68]. The current interruption method is a useful diagnostic tool to measure resistance of an operating fuel cell.

In AC-impedance spectroscopy, the system is perturbed with a small sinusoidal voltage or current signal and the cell impedance can be calculated from the response. Typically the amplitude of the perturbation signal in fuel cell measurements is approximately 10 mV. The impedance data is correlated to cell operation with the aid of an equivalent electronic circuit of the system. Equivalent circuit consists of electronic components, which are used to describe resistive losses, electrode kinetics, and mass transfer. The impedance measurement is normally made on a large frequency range, and different loss mechanisms can be identified due to their different time constants. In Publications I and II AC-impedance spectroscopy was used to evaluate the membrane conductivity and electrode kinetics of the hydrogen oxidation reaction

## **3. Characterization of MEA**

### **3.1. Background**

An MEA is the heart of a PEMFC and its properties affect the performance of the cell significantly. Many properties of MEA depend on its water content. This is one of the reasons why water management and related transport phenomena have a great effect on PEMFC performance and life-time. Important MEA related parameters are e.g. proton conductivity of ionomer phase, diffusion-, hydraulic permeability- and electro-osmotic drag coefficients of water, kinetics of electrode reactions, and water uptake. Knowing these parameters makes the choice of suitable MEA for each application easier and is vital for modeling.

In Publications I and II, the diffusion coefficient of water in the membrane was evaluated with total water flux measurements combined with modeling. Also the conductivity of the membrane was determined as a function of its water content. Measurements were carried out with a symmetrical H<sub>2</sub>-H<sub>2</sub> cell. It has similar components as a PEMFC, and especially the transport phenomena in the polymer membrane are the same. There is no water production in H<sub>2</sub>-H<sub>2</sub> cell and water content of the cell can be accurately controlled by the humidification of inlet gases. This enables direct measurement of diffusive water flux and membrane conductivity under real operating conditions, which is the most important benefit of this method. Water transport by electro-osmotic drag could be studied by adding an external power supply to the system to drive proton current through the membrane. Hydraulic permeation could be investigated by controlling reactant pressures, and applying a pressure gradient over the membrane. However, these were not included in this thesis.

### **3.2. Methods**

#### **3.2.1. Experimental**

Total water flux and impedance measurements were conducted with a symmetrical H<sub>2</sub>-H<sub>2</sub> cell by feeding humidified hydrogen into the cell and measuring the amount of water exiting from each side. The measurement system used and developed in this study is illustrated in Figure 5.

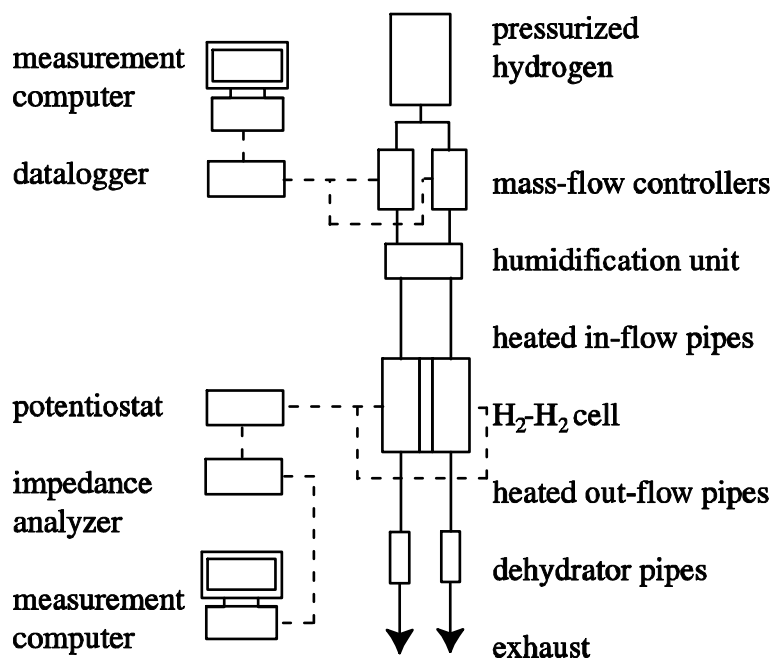


Figure 5. Measurement system used in MEA characterization. Electrical and communication wires are denoted with dashed lines and gas pipes with solid lines.

The humidity levels of ingoing gases on both sides of the cell were controlled independently. The humidity levels of the exhaust gases and the impedance spectrum of the Gore<sup>TM</sup> Primea<sup>®</sup> Series 58 MEA were measured under various humidification conditions. The humidity levels of the exiting gases depend on the water flux through the membrane and therefore can be used to determine the diffusion coefficient of water in the membrane. There was no current going through the cell or pressure difference across the membrane, and therefore water was transported through the membrane only by diffusion.

The conductivity of the membrane and the parameters of reaction kinetics were estimated from the results of impedance measurements. Impedance spectra were recorded with a Zahner IM6 Electrochemical Workstation and PP240 Power Potentiostat. Potential probes were 100  $\mu\text{m}$  thick gold wires attached between the electrodes and PTLs. Potential probes were located outside the active area to avoid disturbing the cell operation.

The structure of the cell is shown in Figure 6. The cell is slightly modified from the one presented in [38, 69]. Flow field plates were made of gold-plated AISI 316 steel net on top of smooth graphite current collectors. Diameters of steel net and current collector were 28 and 30 mm, correspondingly. 1 mm wide free space collected flow from the net, which created radially symmetric flow profile. With traditional channel-type flow field geometry, concentration and velocity profiles would be more complicated and modeling analysis of measurement results harder. Due to cylindrical symmetry, a 2D model can be used as explained in Chapter 3.2.2. With a channel-type flow field geometry 3D analysis would be needed.

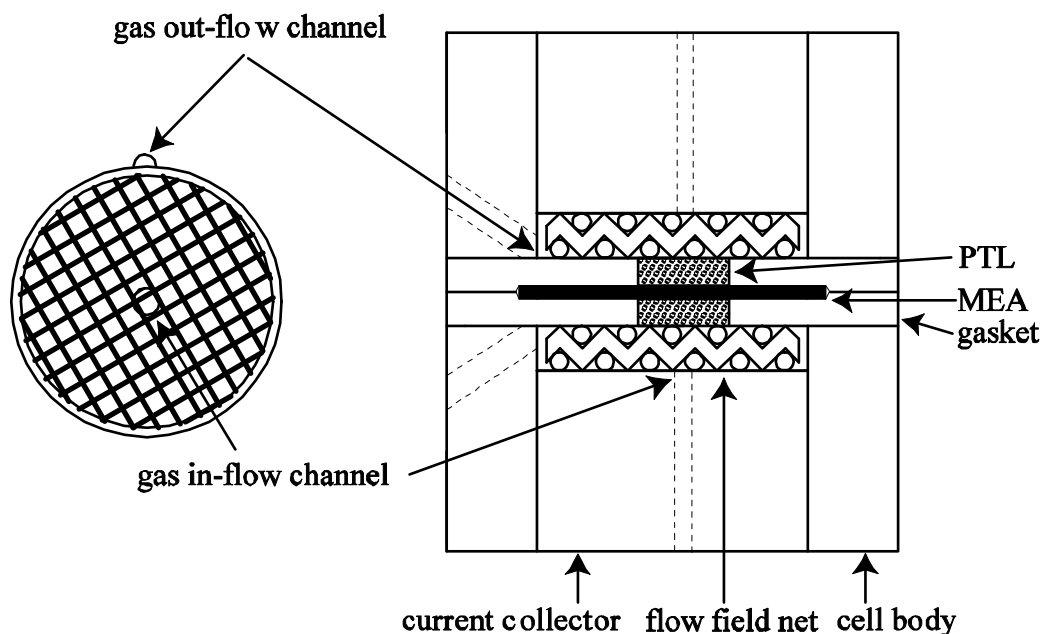


Figure 6. Structure of the cell used in the experiments. Gas channels are marked with dotted line.

Before each measurement, the cell was allowed to stabilize at measurement conditions for at least four hours. Humidity of the inlet hydrogen was varied from dry to dew-point temperatures of 27, 30, 33, 39, and 43 °C. Both sides of the cell were unpressurized and cell temperature was 35 °C.

Impedance measurements were carried out in the frequency range from 500 mHz to 200 kHz. The measurements were conducted in galvanostatic mode with 100 mA amplitude and 0 mA DC-level. The measurement results were analyzed with the equivalent electronic circuit shown in Figure 7. Resistor  $R_1$  describes the pure resistance between the potential probes, which is assumed to be caused by the membrane resistance.  $R_2$  and  $Z_2$  are used to describe the charge transfer processes of adsorbed hydrogen, and they define the high frequency arc of the Nyquist plot.  $R_2$  is the charge transfer resistance and  $Z_2$  is the constant phase element, which is used instead of a normal capacitor because of the capacitance dispersion. Capacitance dispersion is caused by several factors, mainly by electrode roughness, and distribution of reaction rates, see e.g. [70, 71].  $R_3$  and  $C_3$  define the low frequency arc of the Nyquist plot, caused by adsorption and desorption of hydrogen on the electrode surface, see e.g. [66] or alternatively by water transport [72].

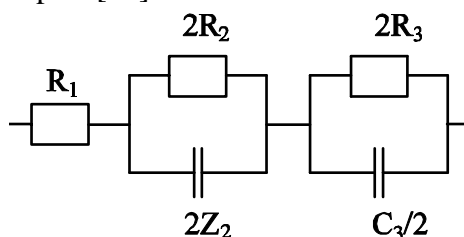


Figure 7. Equivalent electronic circuit for the impedance of H<sub>2</sub>-H<sub>2</sub> cell.

Water uptake of MEA was also measured. Water uptake is an important parameter for the analysis of measurement results, and it describes the equilibrium water content of the sample stabilized with water vapor or liquid water. Before water uptake measurements, MEA samples were dried with P<sub>2</sub>O<sub>5</sub> and weighted. Then they were equilibrated with water vapor or liquid water for at least a week and water uptake was calculated from the weight increase of the sample. In this thesis, water uptake is given as a λ-value (number of water molecules per sulfonic acid group) for easier comparison with reference values. λ-value can be calculated with Equation (7).

$$\lambda = \frac{WU \cdot EW}{M_{H_2O}} \quad , \quad (7)$$

where *WU* is water uptake (mass of water/mass of dry sample), *EW* is the equivalent weight of the sample, and *M<sub>H<sub>2</sub>O</sub>* is the molar weight of water.

### 3.2.2. Modeling

The diffusion coefficient of water in the membrane can not be calculated directly from measured total water fluxes, because the radial distributions of water flux and concentration are not known. Therefore, modeling is essential for the analysis of measurement results.

Reasons for radial distributions of water flux and concentration are presented in Figure 8. Gas enters the flow field net from the center and radially flows outward and exits from the outer boundary. Flow directions of gases are shown in lower subfigure. Water is transported through the PTLs and membrane, which creates a water concentration profile in the radial direction. Concentration profiles of water at membrane surfaces and water flux through the membrane are shown in upper subfigure.

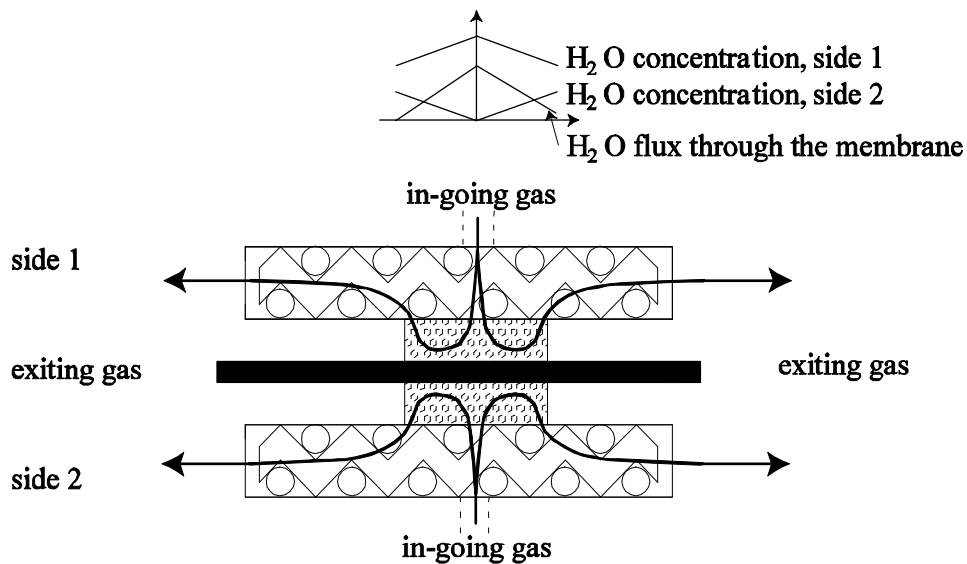


Figure 8. Uneven humidity profile and water flux inside the cell. Components are the same as in Figure 6.

The model developed for the analysis of total water flux measurements includes the transport phenomena of hydrogen and water vapor inside the flow field nets, porous transport layers, and electrodes, and also water transport inside the membrane. Liquid water transport and phase change phenomena are not taken into account, and therefore the model is limited to one-phase conditions. Model geometry is presented in Figure 9. Because the flow geometry of H<sub>2</sub>-H<sub>2</sub> cell used in the measurements is cylindrically symmetric, only half of the cross-section of the cell was modeled.

Hydrogen - water vapor mixture is fed into the cell through the inlet boundaries. Mass transport inside the flow field nets, porous transport layers, and electrodes are described using the Darcy equation for convective transport, the Fick equation for diffusive transport, and the continuity equation. When the membrane surface is in contact with water vapor, water concentration in the membrane near the surface is defined by the water uptake isotherm. The concentration gradient of water across the membrane drives water diffusion through the membrane.

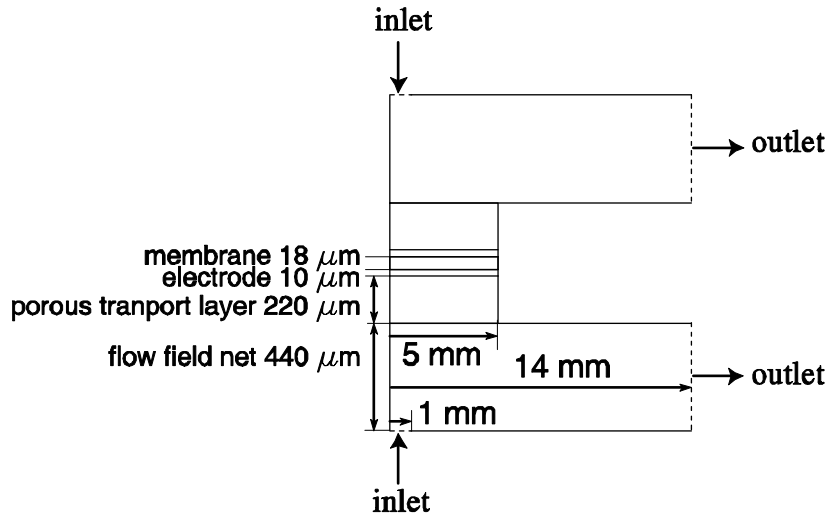


Figure 9. Model geometry. Dashed lines refer to gas inlet and outlet boundaries.

In the total water flux measurements there was no protonic current or pressure gradient across the membrane. Therefore, the only water transport mechanism in membrane is diffusion, which is described by the Fick diffusion equation. There are no water sources or drains in the membrane and therefore the divergence of water flux is zero

$$\nabla \cdot (-D_{\text{H}_2\text{O, membrane}} \nabla c_{\text{H}_2\text{O, membrane}}) = 0, \quad (8)$$

where  $D_{\text{H}_2\text{O, membrane}}$  is the Fick diffusion coefficient of the water in the membrane, and  $c_{\text{H}_2\text{O, membrane}}$  is the concentration of water in the membrane. The diffusion coefficient of water in the membrane was assumed to depend exponentially on the water concentration

$$D_{\text{H}_2\text{O, membrane}} = D_0 \left( 1 - \exp\left(-\frac{c_{\text{H}_2\text{O, membrane}}}{c_{\text{H}_2\text{O, sat}}}\right) \right), \quad (9)$$

where  $D_0$  is the parameter of the model, and  $c_{\text{H}_2\text{O},\text{sat}}$  is the concentration of water in the membrane equilibrated with saturated water vapor. This dependence was developed because it has one free parameter that can be fitted in the model and it gives qualitatively similar behavior as measured for self-diffusion coefficient of water in Nafion<sup>®</sup> 117 in [34].

The model was solved with the Comsol Multiphysics<sup>™</sup> finite element method solver. The parameter  $D_0$  was determined by varying its value until the difference between the modeled and measured concentrations of water vapor at outlets reached its minimum.

A separate model was developed to see if the cell can be treated as an isothermal system also when current passes through the cell, e.g during impedance spectroscopy or electro-osmotic drag measurements. Modeled heat transfer mechanisms were conduction and convection. Heat was produced by activation losses, reaction entropy, water phase change, and resistive losses both in bulk materials and at interfaces.

### 3.3. Results

The measured water uptake of Gore<sup>™</sup> Primea<sup>®</sup> Series 58 MEA is shown in Figure 10. Water uptake from liquid water was measured to be 6.1. Water uptake from liquid water for 20  $\mu\text{m}$  thick Gore-Select<sup>®</sup> membrane has been measured to be 19.5 [5], which is more than three times larger than the value reported here. Water uptake values measured for Nafion<sup>®</sup> 117 membranes reported in [10, 73] are also larger. These values are also shown in Figure 10 for comparison. The difference between reference values and values reported in Publication I is most probably caused by the electrodes. Electrodes are hydrophobic which most probably decreased the water uptake of ionomer in membrane and electrodes. Electrodes also contain platinum and carbon whose water uptake is very small.

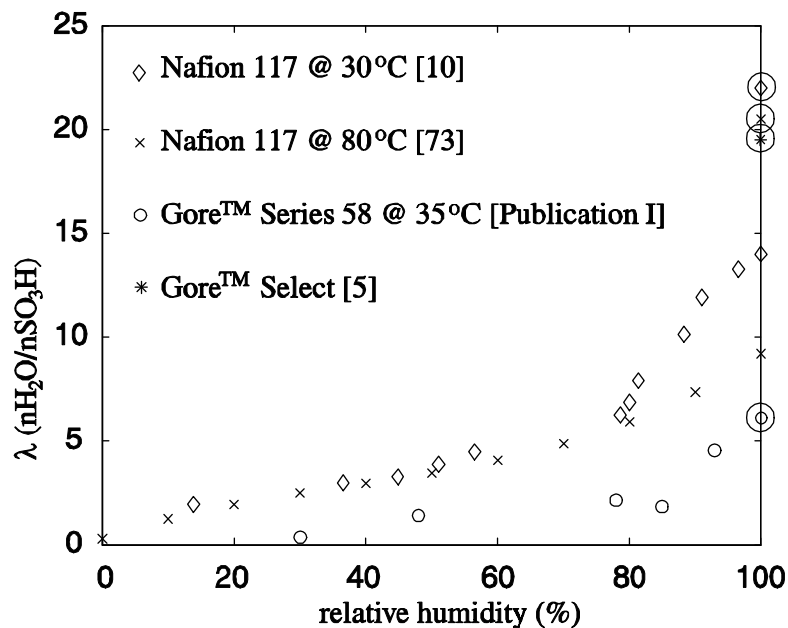


Figure 10. Water uptake of Nafion<sup>®</sup> 117 membrane [10, 73], Gore<sup>™</sup> Select<sup>®</sup> membrane [5], and Gore<sup>™</sup> Primea<sup>®</sup> Series 58 MEA [Publication I]. Water uptake values measured with liquid water are marked with circles.

In the modeling analysis of total water flux measurements, the average difference between measured and modeled outlet concentrations was 3.5%, and the maximum difference was 11%. The value of  $D_0$  was found to be  $1.5 \pm 0.3 \cdot 10^{-9} \text{ m}^2\text{s}^{-1}$ . The resulting Fick diffusion coefficient of water in the membrane is given in Figure 11.

Three different equations for the Fick diffusion coefficient of water in Nafion<sup>®</sup> are given in the literature [53] based on the work by various groups [10, 52, 74]. These diffusion coefficients are also shown in Figure 11 for comparison.

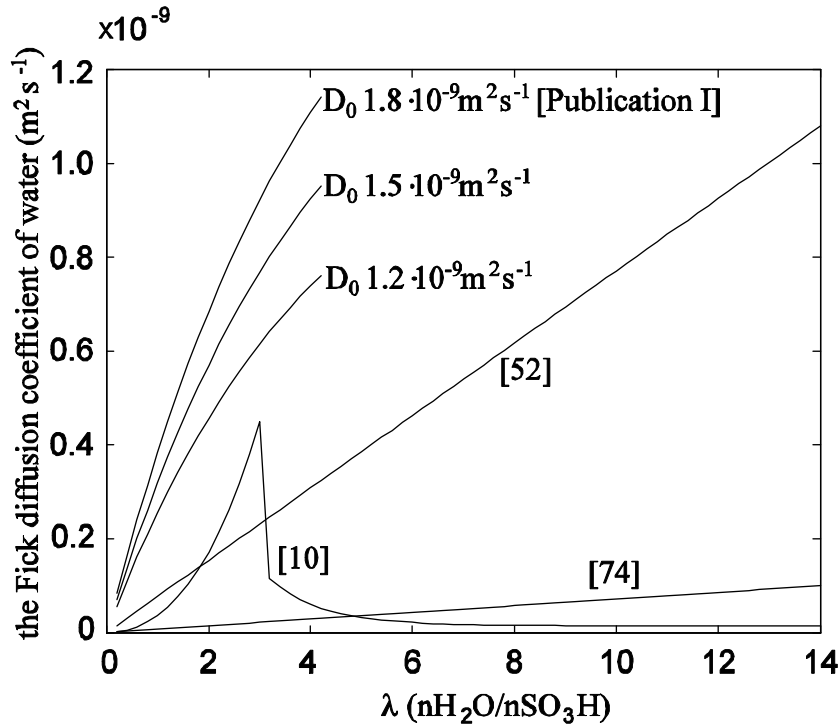


Figure 11. The Fick diffusion coefficient of water in the membrane as a function of membrane water content.

Diffusion coefficient values reported here for Gore<sup>™</sup> Primea<sup>®</sup> Series 58 MEA are larger than the literature values for Nafion<sup>®</sup> membrane. The diffusion coefficient was determined in Publications I and II using the whole MEA under realistic operating conditions of fuel cell. The electrode layer affected the water uptake measurements and most probably decreased water uptake values. Smaller water uptake values lead into smaller concentration gradient of water in the membrane. The net water flux through the membrane in the model was set to the measured value and smaller concentration gradient led into overestimation of diffusion coefficient. One can roughly estimate that diffusion coefficients should be approximately three times smaller than the values reported here, because water uptake values were three times larger than the values reported in the literature. However, the values of diffusion coefficient and water uptake reported here give the correct water flux through the membrane, but they must be used together. It would be very useful to measure water transport and water uptake properties also with plain membrane used in Gore<sup>™</sup> Primea<sup>®</sup> Series 58 MEA. Then it might be possible to separate the effects of the electrodes and membrane.

As explained in Chapter 3.2.2. modeling analysis is very important for this characterization method, when there is uneven water concentration profile inside the cell. An example of this is given in Figure 12, which shows the modeled concentration profile inside the test cell. The humidity conditions refer to the measurement where the dew-point temperature of inlet gas on side 1 was 33.4 °C and on side 2 it was dry. Water vapor concentration differences along the membrane surface are large and lead into significant lateral variation of water flux through the membrane. Only some kind of average diffusion coefficient could be obtained from the measured total water flux without modeling.

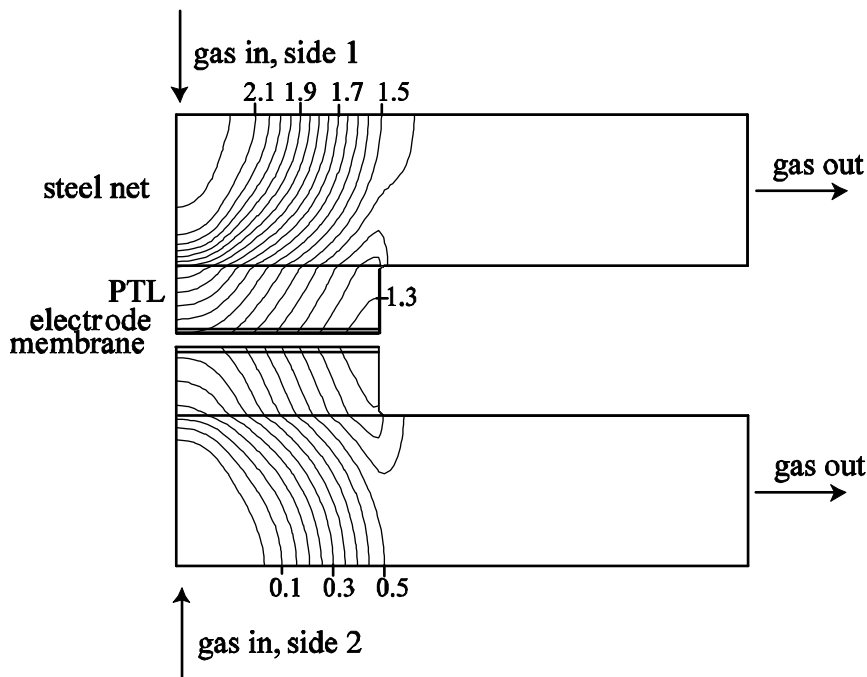


Figure 12. Modeled water concentration distribution inside the test cell. Contours refer to water concentration ( $\text{mol m}^{-3}$ ).

The conductivity of the membrane was evaluated from the results of impedance measurements by fitting the component values of equivalent circuit into the results. The resulting conductivity of the membrane as a function of water vapor concentration is given in Figure 13. The conductivity of the membrane in contact with liquid water was found to be  $5.3 \pm 0.1 \Omega^{-1} \text{ m}^{-1}$ . This value is in good agreement with the  $5.2 \Omega^{-1} \text{ m}^{-1}$  measured for 20  $\mu\text{m}$  thick Gore-Select<sup>®</sup> membrane in [5].

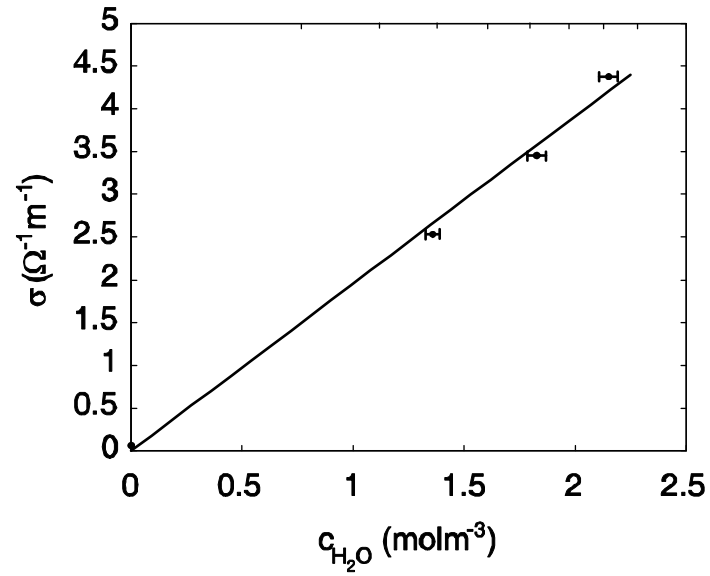


Figure 13. Conductivity of the membrane as a function of water vapor concentration

The temperature distribution inside the cell was studied by modeling. Even at a  $0.7 \text{ A cm}^{-2}$  current density, the maximum temperature variation inside the cell was less than  $1 \text{ }^\circ\text{C}$ . Most of the temperature differences occurred at interfaces between different components. Temperature differences inside bulk material were less than  $0.1 \text{ }^\circ\text{C}$ . The result shows that the  $\text{H}_2\text{-H}_2$  cell can be treated as an isothermal system, even at relatively high current densities, e.g. with electro-osmotic drag measurements.

## **4. Water Management of a Free-Breathing PEMFC under Various Operating Conditions**

### **4.1. Background**

Free-breathing PEMFC is in close contact with ambient air and has to operate under different humidity and temperature conditions. Due to passive controlling methods and varying ambient conditions, knowledge of water management and other transport phenomena in free-breathing PEMFC are vital for their development and design. Here the operation of a free-breathing PEMFC was investigated in dead-end mode and at low temperatures (-27.5 °C – 0 °C). Reduced water removal with exiting hydrogen in dead-end operation makes the water management of the cell more complicated compared to normal flow-through mode. Water management is a very important and challenging issue at subzero temperatures, because of possible freezing of water inside and outside the cell.

The effect of low temperature on the operation of PEMFC has been studied in several articles. Cho et al. [75, 76] studied different water removal methods and antifreeze solutions to decrease freezing of water inside the cell. Hou et al. [77] studied the freeze degradation with different water removal methods. Cold start behavior of the PEMFC has been studied by several groups [78-84]. They found that the cell has to be dried prior to cooling and possibly heated before start-up. Without these measures irreversible performance loss will occur. However, to the knowledge of the author, Publication IV is the first published study made with a free-breathing PEMFC.

The operation of a free-breathing PEMFC was tested in dead-end mode. Dead-end operation is commonly used in commercial PEMFC systems because it enables high fuel utilization rate. In dead-end mode, anode side of the cell is pressurized and hydrogen outlet is equipped with purge valve to flush the anode periodically. Purging removes excess water and inert gases from the anode side. The operation of the cell was investigated at different hydrogen pressures and purge rates by constant current and polarization measurements. There are a few studies where the operation of PEMFC in dead-end mode has been studied [85-88]. In addition to Publication III, the author could not find any other studies made with a free-breathing PEMFC.

### **4.2. Methods**

#### **4.2.1. Sub-Zero Tests**

The test cell was similar to one presented in Figure 2. Anode and cathode current collectors were made of gold-coated SS316 steel. Anode flow channel was Z-shaped, depth and width of the channel were 1 mm and 3 mm, respectively. Cathode current collector had 2 mm wide openings and 1 mm ribs. Porous transport layers were SGL SIGRACET® 10BC. The MEA was Gore® Primea™ Series 55.

Measurement system used in sub-zero tests is shown in Figure 14. The fuel cell test station was GlobeTech GT-100. The fuel cell was placed inside a temperature chamber

(modified Electrolux EC1109N). Temperature of the cell was measured with two Pt-100 sensors located on the cathode current collector. Pressure of gas going into the cell was measured with Brooks 5866 pressure controller. The temperature chamber was also equipped with a digital camera to get visual information on ice formation onto the cathode structure of the cell.

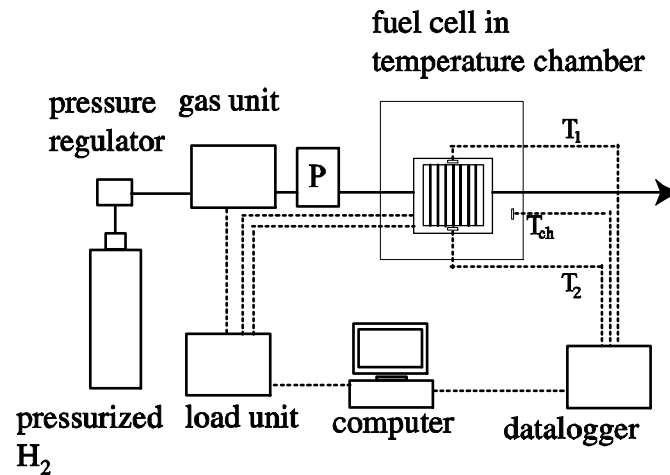


Figure 14. Measurement system used in sub-zero tests. Gas pipes are drawn with solid line and electrical and communication wires with dashed line. T<sub>1</sub>, T<sub>2</sub>, and T<sub>ch</sub> are temperature sensors. P refers to pressure meter.

The operation of the cell at sub-zero temperatures was investigated with constant current and cold-start measurements. In constant current measurements, the cell was first operated at room temperature and then the temperature of the chamber was decreased to the desired temperature. Constant current measurements were made at temperatures between 0 °C and -27.5 °C. The value of the current was varied from 200 to 600 mA cm<sup>-2</sup> depending on the temperature.

Cold-start of the cell was tested at -5 and -10 °C. Before cooling down, the cell was dried at room temperature. Cathode side of the cell was dried with air pulse from a compressed air line and the anode side was flushed with nitrogen. After this drying procedure, the chamber was cooled to the desired temperature and allowed to stabilize for more than 12 hours. After this the hydrogen flow was turned on and the cell was started. At -5 °C the current density was increased from 0 to 200 mA cm<sup>-2</sup> and at -10 °C to 300 mA cm<sup>-2</sup> in 17 mA cm<sup>-2</sup> steps. The time intervals between current increases were 30 s and 60 s.

To reveal possible irreversible performance losses due to freezing, a polarization curve was measured after every constant current and cold-start measurement. This curve was compared to a reference curve measured before the measurement series. If the polarization measurement showed changes in the cell performance, the MEA and PTLs were replaced.

#### 4.2.2. Dead-End Tests

The operation of a free-breathing PEMFC was tested in a dead-end mode with the measurement system illustrated in Figure 15. The measurement system consisted of the

same gas and load units as in sub-zero tests. Here the gas unit was used to measure the hydrogen flow rate, not to control it. A Bürkert 6013 solenoid valve was located downstream from the cell and acted as a purge valve. Upstream from the cell was a Brooks 5866 pressure controller, which was used to adjust the pressure of hydrogen inside the cell. Between the gas unit and pressure controller was a needle valve, which limited the hydrogen flow rate and pressure peaks during and after the purge. The fuel cell was similar to the one used in sub-zero tests, except the MEA was Gore<sup>TM</sup> Primea<sup>®</sup> Series 58.

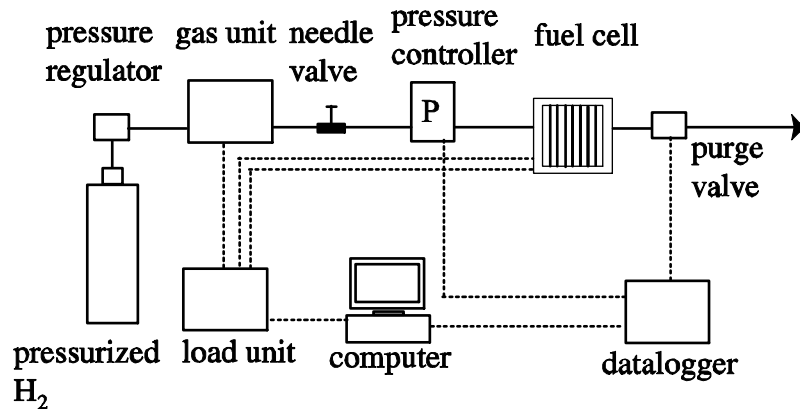


Figure 15. Measurement system used in dead-end tests. Gas pipes are drawn with solid line and electrical and communication wires with dashed line.

Two different hydrogen pressure levels, 0.1 and 0.25 barg were used in these tests. Both dry and humidified hydrogen with dew-point temperature of 30 °C were used to simulate hydrogen provided from high pressure or chemical hydride storage. The cell was unheated, but the needle valve, pressure controller, and gas pipes were heated to 35 °C to avoid condensation of water vapor in the gas line. Duty cycle of the purge valve was varied from completely closed to 1/60, 1/120, 1/300, 1/600, and 1/1200 seconds open / seconds closed. Optimum values of parameters like hydrogen pressure and the valve open time depend on the application and operating point and were not optimized here.

At each humidity and pressure level, and purge valve duty cycle, polarization and constant current measurements were performed. Polarization curves were measured three times consecutively to minimize the effect of load history. In constant current measurements, the cell current was kept at 1.5 A (250 mA cm<sup>-2</sup>) for 8 hours and the cell voltage was recorded during that period. In addition to these dead-end measurements, reference measurements were also conducted in a flow-through mode with a stoichiometry of 1.5. Dew-point temperature of hydrogen in reference measurements was 30 °C.

### 4.3. Results

#### 4.3.1. Sub-Zero Tests

Sub-zero tests showed that a free-breathing PEMFC is able to operate at very cold temperatures if the current density and thus the heat production are high enough to

avoid internal freezing of the cell. If the heat production was not high enough, reaction product water froze inside the cell and caused irreversible performance losses. An example of the effects of irreversible losses on the polarization behavior of the cell is illustrated in Figure 16. The polarization curve marked with “-15 °C” was measured after the 300 mA cm<sup>-2</sup> constant current measurement at -15 °C. The reference curve was measured before the measurement series. The cell performance is significantly lower due to increased resistive and mass transfer losses. This was most probably caused by the partial detachment and structural changes of various components. After the similar test with 400 mA cm<sup>-2</sup> constant current at -15 °C, irreversible performance losses were not observed due to larger heat production.

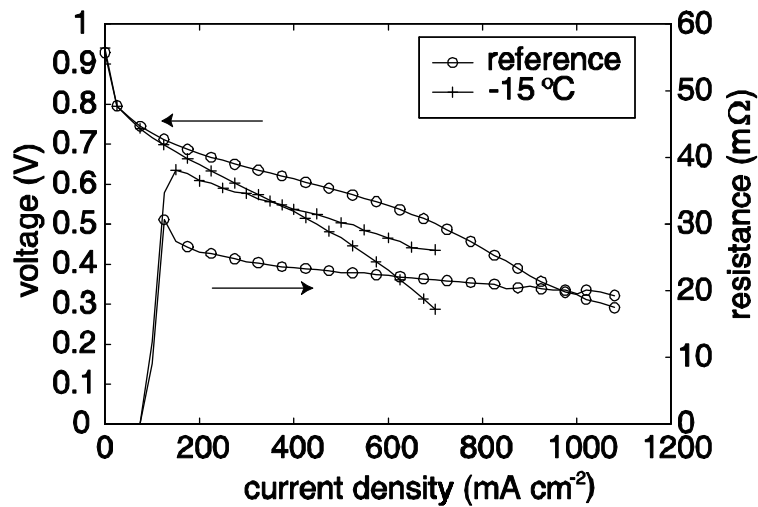


Figure 16. Polarization and resistance curves after the measurement at -15 °C with 300 mA cm<sup>-2</sup> and reference curves before the measurement series.

The performance of the cell decreased when the temperature was decreased. This was most probably because of decreased reaction kinetics and increased mass transfer limitations. Mass transfer limitations were caused by ice formation on the cathode side but it was partly compensated with increased convection due to larger temperature difference between the cell and ambient air. The lowest measured temperature was -27.5 °C, where the cell was operated at 600 mA cm<sup>-2</sup> average current density. At this temperature the cell performance decreased significantly, the cell voltage was 0.35 – 0.45 V with approximately 60 mV fluctuations. There was a lot of frost and ice formation on the cathode surface during this measurement, increasing the mass transfer losses. Cell voltage and resistance from this measurement are presented in Figure 17 and frost formation in Figure 18.

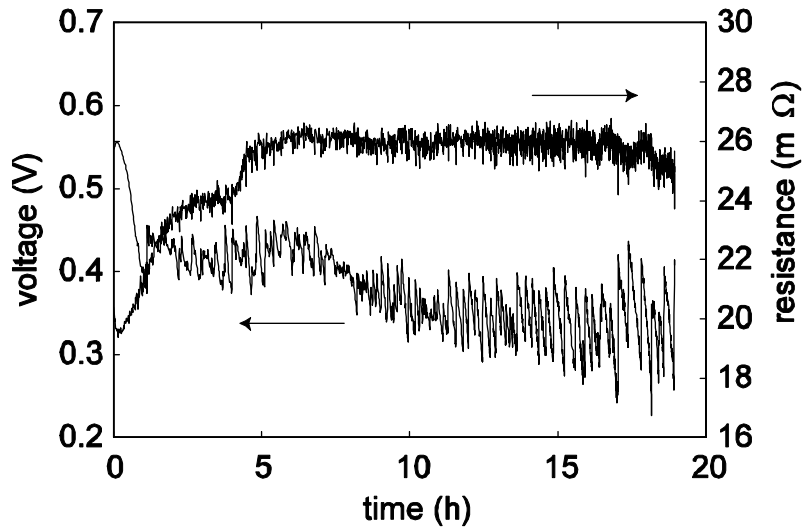


Figure 17. Cell voltage and resistance at  $-27.5\text{ }^{\circ}\text{C}$  with  $600\text{ mA cm}^{-2}$ .

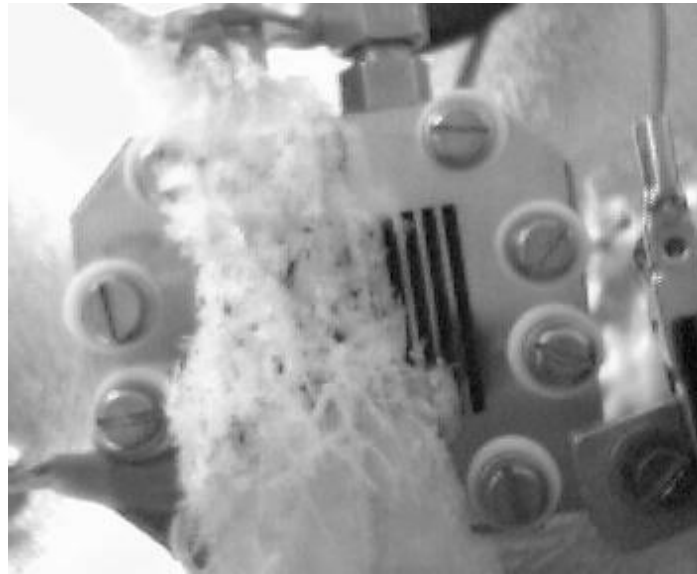


Figure 18. Frost and ice formation on the cathode surface at  $-27.5\text{ }^{\circ}\text{C}$ .

During some constant current tests, the reaction product water froze inside the exhaust pipe and blocked the hydrogen exit and the cell started to operate in a dead-end mode. The maximum hydrogen pressure was 2.7 barg, which showed that the cell is able to withstand high pressure differences at least short periods of time without irreversible performance losses.

The initially dry cell was able to start at  $-5\text{ }^{\circ}\text{C}$  with 30 s and 60 s intervals between current steps without any problems. The final current density at  $-5\text{ }^{\circ}\text{C}$  was  $200\text{ mA cm}^{-2}$ . At  $-10\text{ }^{\circ}\text{C}$  the target current density was larger,  $300\text{ mA cm}^{-2}$  to avoid freezing of reaction product water inside the cell. At  $-10\text{ }^{\circ}\text{C}$  with current increase every 30 s, the cell current density increased to  $233\text{ mA cm}^{-2}$  after which the voltage collapsed. With current increase every 60 s, the cell started up without problems, but some irreversible

performance losses occurred. The problems occurred at  $-10\text{ }^{\circ}\text{C}$  were most probably caused by the freezing of the reaction product water inside the cell. The cell voltage and temperature during the cold-start tests are shown in Figure 19.

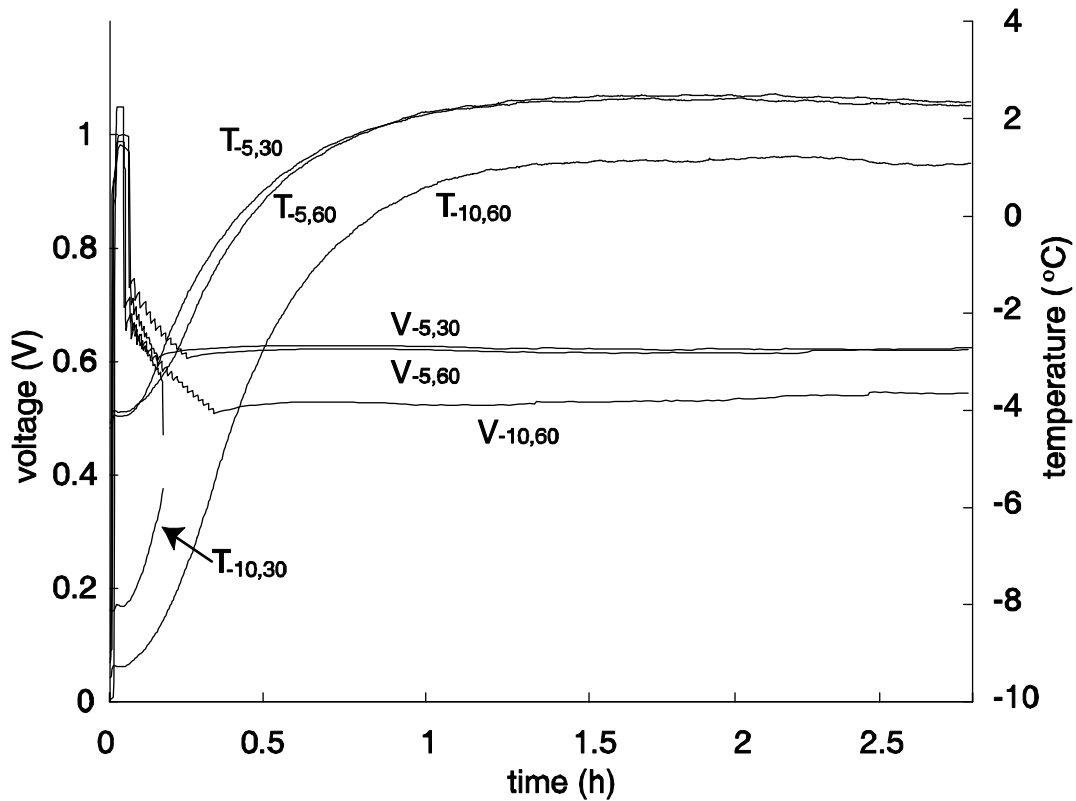


Figure 19. Cell voltage and temperature during cold-starts. Subscript notation: initial temperature, time interval between current increases

#### 4.3.2. Dead-End Experiments

Polarization curves measured at 0.1 and 0.25 barg hydrogen pressure showed that the cell performance practically does not depend on the purge rate, as long as the purge valve is periodically opened. With the purge valve completely closed, the performance decreased slightly and the polarization scan had to be reversed at 0.5 V due to instable operation of the cell. This instability was most probably caused by water accumulation in the anode side at high current densities.

The humidity of the hydrogen had no effect on the cell polarization behavior when the anode side was purged periodically. When the purge valve was closed, the performance of the cell was slightly weaker with humidified hydrogen, again due to increased water accumulation on the anode side of the cell.

At 0.25 barg hydrogen pressure, the cell performance at high current densities was slightly weaker than in the reference measurements or at 0.1 barg pressure. Higher hydrogen pressure increased the water transport from the anode to cathode by hydraulic permeation. This led to excess water at the cathode side of the cell, which decreased cell performance. The polarization curves measured at 0.25 barg are presented in Figure 20.

For clarity, measurement results with 1/120, 1/300, and 1/600 duty cycles are not shown, but they fell between the extreme cases presented here.

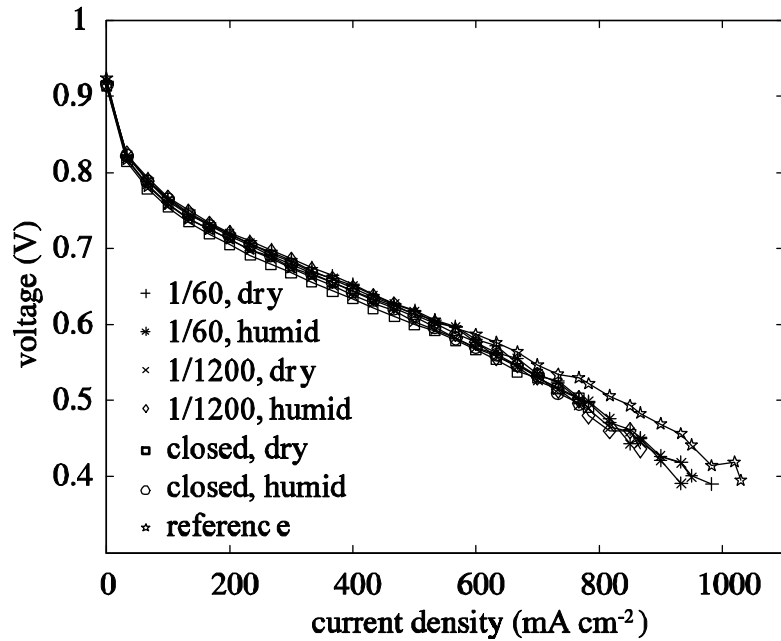


Figure 20. Polarization curves measured at 0.25 barg hydrogen pressure

Constant current measurement supported the observations made with polarization curve measurements. Cell performance did not depend on the duty cycle of the purge valve or on the humidity of hydrogen as long as the valve was periodically opened. At 0.1 barg pressure and purge valve closed the cell voltage started to decrease after 6 hours with dry hydrogen and after 4 hours with humid hydrogen. At 0.25 barg pressure this did not happen. This implies that the higher hydraulic permeation at 0.25 barg, decreased the flooding of the anode. The results of constant current measurements made at 0.1 barg hydrogen pressure are shown in Figure 21. Again the three middle duty cycles were omitted.

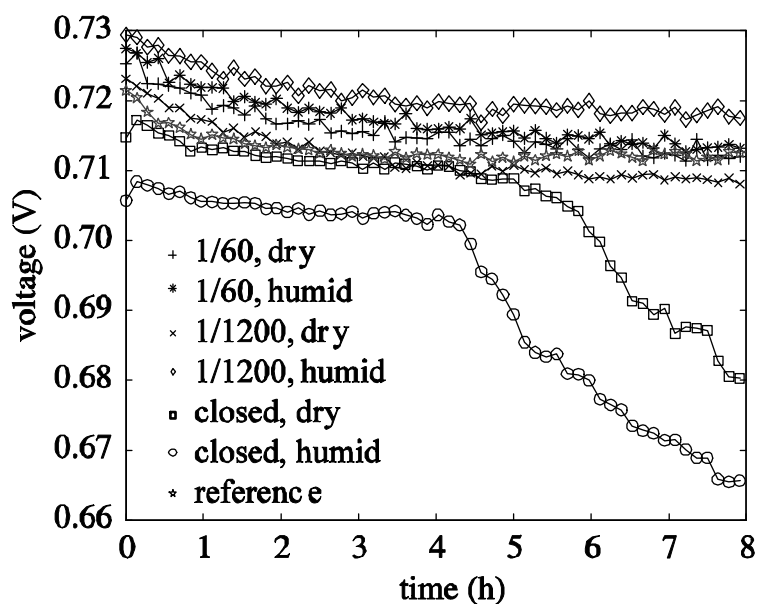


Figure 21. Cell voltage during constant current measurements, hydrogen pressure 0.1 barg.

Hydrogen consumption due to purging was measured to evaluate the fuel utilization rate. Measured hydrogen flow rate is presented in Figure 22. Duty cycle of the purge valve was 1/1200, hydrogen was dry and pressure was 0.1 barg. The average fuel utilization rate calculated over 1200 s period was 0.95. Higher fuel utilization rates should be possible by optimizing the purge parameters, because the operation of the cell was quite stable even with completely closed purge valve.

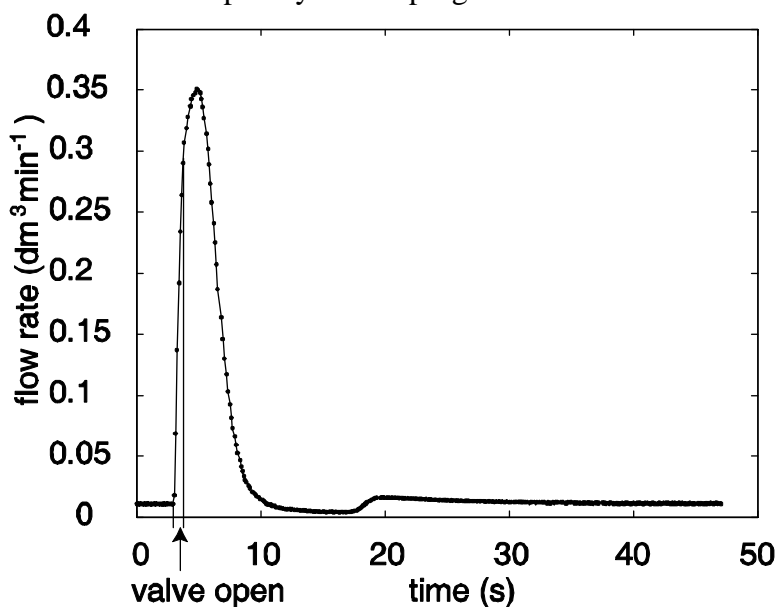


Figure 22. Hydrogen flow rate during purge.

## 5. Inhomogeneous Compression of Porous Transport Layer

### 5.1. Background

When a PEMFC is assembled, porous transport layer is compressed between the flow field plate and electrode. Due to the channel-rib structure of traditional flow field plates, the compression is inhomogeneous. Most of the compression force is directed to PTL located under the ribs, but the areas under the channels remain almost uncompressed, see Figure 23.

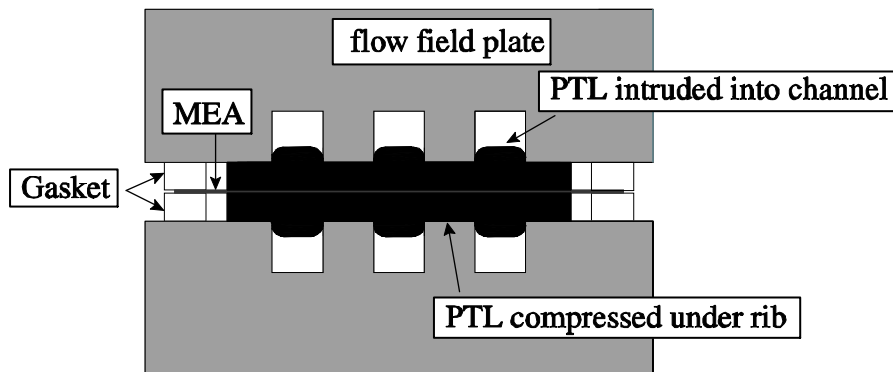


Figure 23. Inhomogeneous compression of PTL

Many bulk and interfacial properties of PTL depend on its compressed thickness and inhomogeneous compression causes spatial variation of these parameters and affects the transport phenomena inside the cell.

In Publication V, PTL intrusion into channel, gas permeability, electrical conductivity and contact resistance were evaluated as a function of compressed thickness. Parameters were evaluated as a function of compressed thickness instead of compression pressure, because thickness dependence is more useful in modeling. Also when a PEMFC is assembled, the compressed thickness of PTL is fixed by gaskets. Experimentally evaluated parameter values were used in Publications VI and VII in a computer model, which was developed to see the effects of inhomogeneous compression on PEMFC operation and transport phenomena.

There are several articles where the inhomogeneous compression of PTL is studied. Sun et al. [89] and Zhou et al. [90] published models where some of the effects of inhomogeneous compression were taken into account. Freunberger et al. [91] were able to measure the current distribution with sub millimeter resolution at the PTL-electrode interface and also studied the deformation of PTL experimentally and with structural mechanical calculations.

## 5.2. Experimental

### 5.2.1. PTL Intrusion into Channel

The intrusion of PTL into channel was studied with the experimental setup illustrated in Figure 24. PTL sample was located between two aluminum plates whose distance was controlled with steel gages. When the aluminum plates were compressed against each other, the PTL sample partly intruded into the groove in one aluminum plate. Intrusion depth was measured with a dial indicator. Thickness of the steel gages and thus the thickness of the compressed PTL was varied from 150 to 350  $\mu\text{m}$ . Width of the groove was varied from 0.6 to 2 mm.

The PTL used in all measurements was SGL SIGRACET<sup>®</sup> 10BA. Its uncompressed thickness is 380  $\mu\text{m}$ , it has no microporous layer, is treated with 5 wt% PTFE and has porosity of 0.88 [92]. All measurements were repeated several times to minimize the effect of variation in the uncompressed thickness of 10BA.

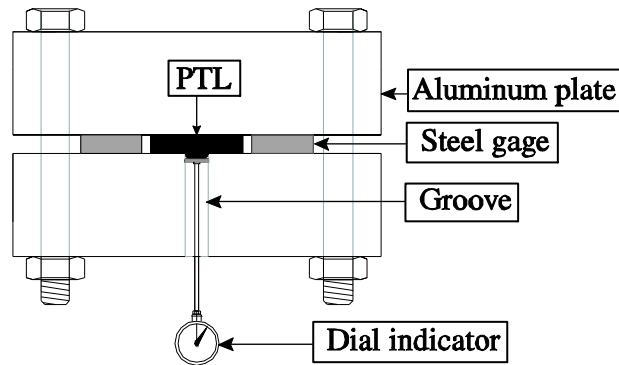


Figure 24. Experimental setup for PTL intrusion measurement

### 5.2.2. Gas Permeability

In-plane gas permeability of PTL was measured with a measurement device presented in Figure 25. A circular PTL sample was located between two aluminum plates. The compressed thickness of the PTL was controlled with steel gages located between the plates. Dry air flowed through the sample radially outwards from the center and the air pressure at the inlet was measured. The gas permeability was calculated using the Darcy equation and the pressure difference over the sample.

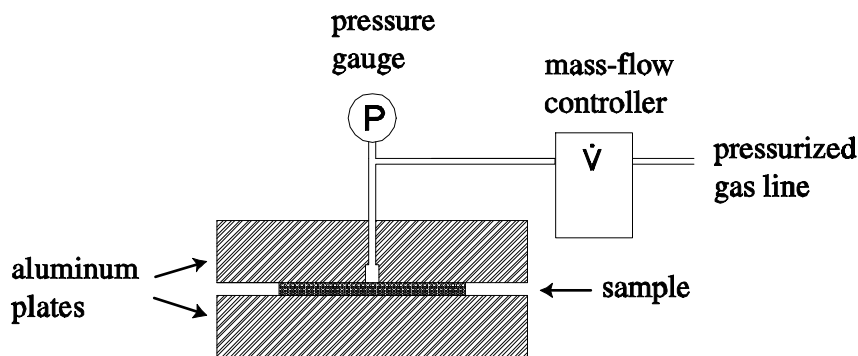


Figure 25. Measurement system for gas permeability

### 5.2.3. Electrical Conductivity and Contact Resistance

Experimental system used for through-plane conductivity measurements is shown in Figure 26. From one to six PTL samples were sandwiched between two graphite plates and the resistance between graphite plates was measured. The thickness of PTLs was again controlled with steel gages.

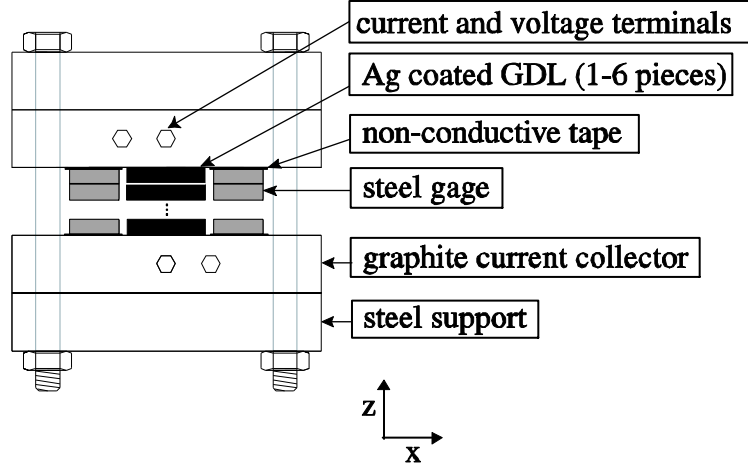


Figure 26. Measurement system for through-plane electrical conductivity.

The total resistance between voltage terminals with different number of PTL samples can be expressed as

$$R = 2 \cdot R_{gr,bulk} + n \cdot R_{PTL,bulk} + 2 \cdot R_{PTL-gr,cont} + (n - 1) \cdot R_{PTL-PTL,cont} , \quad (10)$$

where  $R$  is the total resistance,  $R_{gr,bulk}$  is the resistance of graphite current collector,  $R_{PTL,bulk}$  is the bulk resistance of one PTL,  $R_{PTL-gr,cont}$  is the contact resistance between current collector and PTL,  $R_{PTL-PTL,cont}$  is the contact resistance between PTLs, and  $n$  is the number of PTL samples. Bulk resistance of graphite remains constant, but the other three parameters depend on compression and the direct differentiation of their contributions is very challenging.

Here the contact resistance between PTLs was minimized by applying a silver coating. Those surfaces that were in contact with other PTLs were coated, but surfaces that were in contact with graphite were left uncoated. The thickness of the coating was 150 nm and it was made by sputtering. It has been shown that this kind of coating reduces the contact resistance significantly [93, 94], but due to small penetration it does not change the bulk conductivity [95]. Silver sputtering was measured to decrease the total resistance approximately 10% compared to uncoated samples. Therefore, the contact resistance between PTL samples was assumed to be negligible. The accuracy of this assumption should be studied in the future. The bulk resistance of PTL is the slope when one plots  $R$  as a function of  $n$ . The through-plane conductivity of PTL was then calculated from the bulk resistance.

The contact resistance between PTL and graphite was evaluated with the same measurement system as the bulk conductivity of PTL. When the bulk conductivity of

PTL and graphite are known and PTL-PTL contact resistance is neglected, the only unknown variable in Equation (10) is the contact resistance between PTL and graphite. Due to uneven current distribution in the measurement system, the potential profile through the measurement system was modeled with COMSOL Multiphysics 3.2a, and the contact resistance between PTL and graphite was varied until the total resistance given by the model matched the experimental results. This was done with different number of PTLs and with different compressed thicknesses.

The in-plane conductivity of PTL was measured with an experimental setup illustrated in Figure 27. PTL sample is located on a non-conducting base plate. Both ends of the PTL are compressed under graphite current collectors. Steel gages were installed between the base plate and current collectors to fix the thickness of PTL under the current collectors to 250  $\mu\text{m}$ . The distance between current collectors was varied from 1 to 32 mm. The part of PTL between the current collectors was compressed with a plastic plate and the compressed thickness was varied with steel gages from 150 to 250  $\mu\text{m}$ .

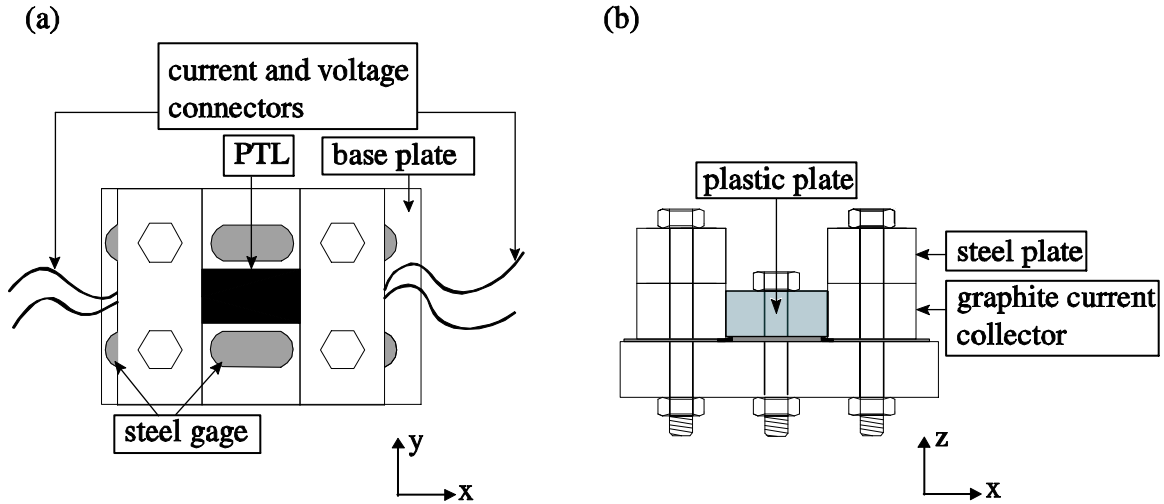


Figure 27. Measurement system for in-plane conductivity. (a) top-view, (b) side-view

The total resistance between the graphite plates,  $R$ , can be expressed as

$$R = 2 \cdot R_{\text{gr,bulk}} + 2 \cdot R_{\text{PTL-gr,cont}} + 2 \cdot R_{\text{PTL,bulk}(250)} + R_{\text{PTL,bulk}}, \quad (11)$$

where  $R_{\text{gr,bulk}}$  is the resistance of graphite current collector,  $R_{\text{PTL-gr,cont}}$  is the contact resistance between PTL and graphite plates,  $R_{\text{PTL,bulk}(250)}$  is the resistance of PTL under the graphite plate, and  $R_{\text{PTL,bulk}}$  is the resistance of PTL between graphite plates. When the distance between current collectors is varied, the change in  $R$  is caused by the change in  $R_{\text{PTL,bulk}}$ , while all other parameters are assumed to remain constant. Varying the compressed thickness of PTL between current collectors, the in-plane conductivity of PTL can be calculated.

### 5.3. Modeling

Due to the small scale, experimental investigation of the effects of inhomogeneous compression on local PEMFC operation and transport phenomena is very challenging. Therefore these effects were studied by modeling using the measured parameter values in the model. The original model used in Publication VI was isothermal and in Publication VII it was modified to be non-isothermal. Here only the non-isothermal model is described, because the models were mostly identical.

Two different cases were modeled, a “base case” where the properties of PTL were assumed to be homogeneous and a “real case” where the effects of inhomogeneous compression were taken into account. The model took into account charge, heat and multicomponent mass transfer in cathode PTL and electrode. Mass transfer was not modeled in the membrane or in the anode PTL or electrode. Two-phase effects were neglected except the loss of porosity due to liquid water.

The modeled geometry is shown in Figure 28. Due to symmetry, only a half of the repeated channel/rib structure was modeled. For simplicity, the intrusion of PTL into anode gas channel was neglected in the modeled geometry. However, the electrical and thermal properties of the anode PTL were calculated by taking the inhomogeneous compression into account.

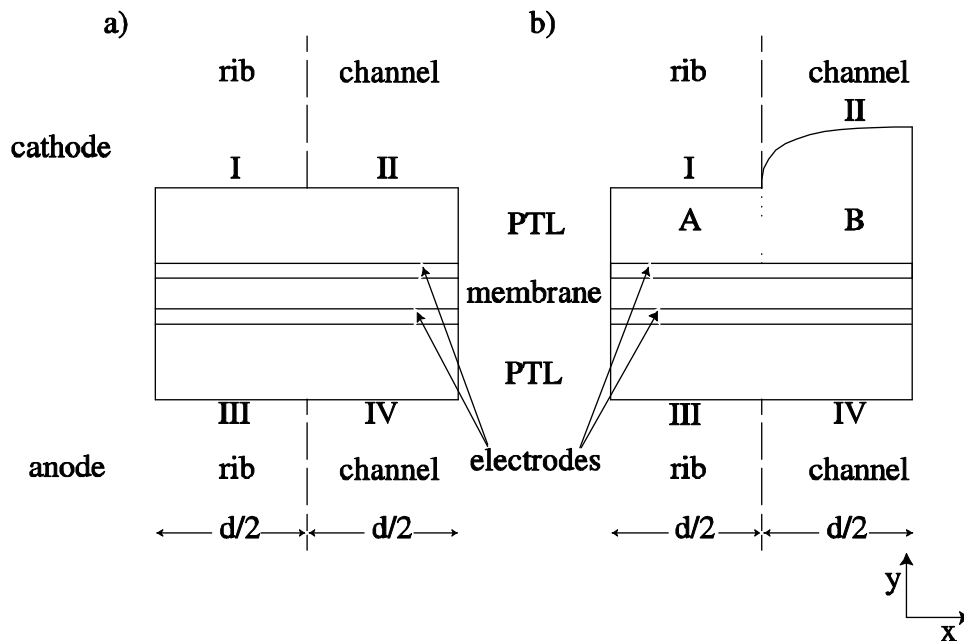


Figure 28. Modeled geometry. a) "base case" inhomogeneous compression neglected, b) "real case" inhomogeneous compression taken into account.

Multicomponent mass transfer takes into account both convective Darcy flow and Maxwell-Stefan diffusion. The rate of electrochemical reactions at the cathode was calculated using Equation (3). The heat was assumed to be transferred by conduction and convection and produced by resistive and activation losses and reaction entropy

production. The contacts between different components were modeled as 0.5  $\mu\text{m}$  layers, whose conductivities were calculated from contact resistances.

## 5.4. Results

### 5.4.1. Experimental

Measured PTL intrusion into channel is presented in Figure 29. Uncompressed thickness given by the manufacturer, 380  $\mu\text{m}$ , was used. Measurements were repeated several times to minimize the effect of thickness variation. The channel width and thickness of steel gages, i.e. compressed thickness of PTL were varied, but the maximum thickness of PTL under the channel remained close to its original thickness. In later experiments, this phenomenon was studied with optical microscopy [96] and one of the microscopy images is given as Figure 30.

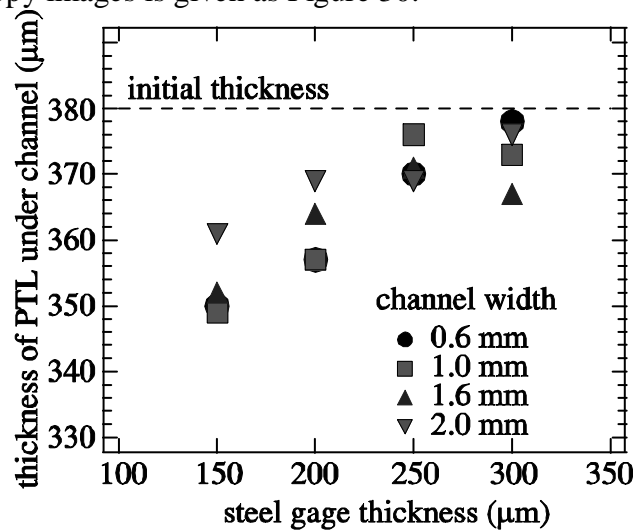


Figure 29. PTL intrusion into channel.

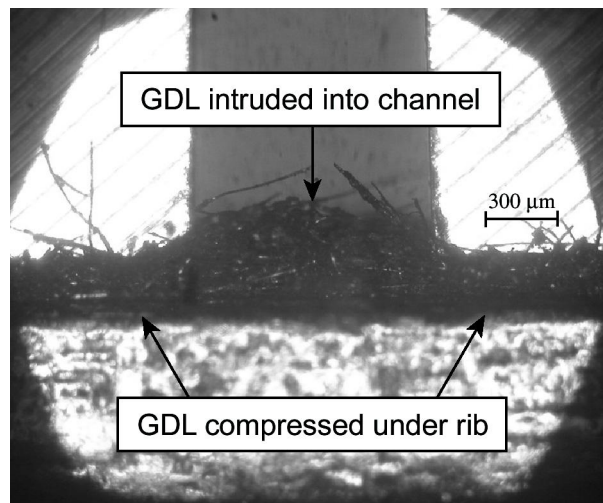


Figure 30. Deformation of PTL under the channel-rib structure, modified from [96].

Measured in-plane gas permeability of PTL as a function of its compressed thickness is given in Figure 31. The gas permeability varied non-linearly as a function of compressed thickness. The measured permeability values are in agreement with the values reported in the literature, e.g. [35, 97]. The results show that the difference in gas permeability between uncompressed PTL under the channel and compressed PTL under the ribs can be as large as one order of magnitude.

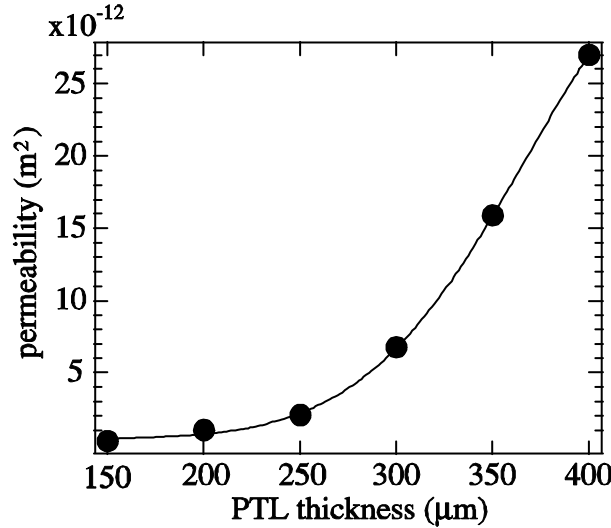


Figure 31. In-plane gas permeability of PTL as a function of compressed thickness

The values of in-plane and through-plane conductivities of PTL as a function of thickness are illustrated in Figure 32. The conductivity values are averaged from several measurements and the error estimates are calculated from standard deviation. In-plane conductivity of PTL was significantly larger than the through-plane conductivity, most probably due to the in-plane orientation of carbon fibers in the PTL. Literature values for in-plane conductivity of PTL vary from 5000 to 23000  $\text{Sm}^{-1}$  [35, 38, 98, 99] and for through-plane conductivity from 300 to 1400  $\text{Sm}^{-1}$  [35, 92, 100, 101]. Large variations can be explained with different PTL materials and measurement techniques, but also with the drawbacks in measurement setups and assumptions.

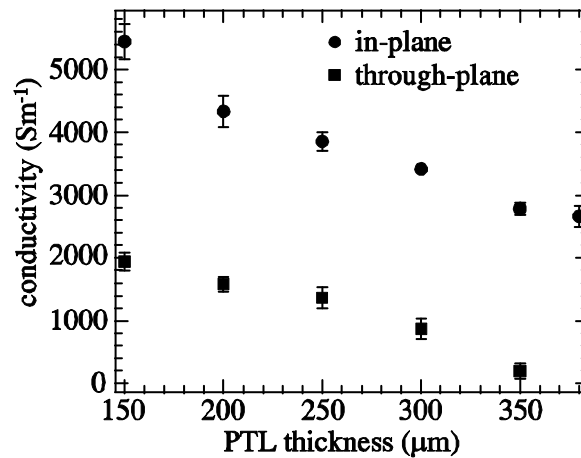


Figure 32. In- and through-plane conductivity of PTL.

The contact resistance between graphite and PTL and its error estimates are shown in Figure 33. Error estimates are calculated by taking the error estimates of bulk conductivity into account in the modeling. Literature values for PTL-graphite contact resistance vary from 1 to 50  $\text{m}\Omega \text{ cm}^{-2}$  with compression pressure from 0.5 to 2 MPa [35, 90, 99, 100-102]. This large variation is most probably related to different materials, but possibly also caused by underestimation or ignoring the contribution of bulk resistance of current collectors due to their high conductivity. The conductivity of isotropic ISEM-3 graphite used in this work was measured to be  $69700 \pm 300 \text{ Sm}^{-1}$ , which is more than one order of magnitude larger than the conductivity of PTL. However, the current path in current collector is typically much longer than the PTL thickness and therefore their resistances are of the same order of magnitude and cannot be neglected.

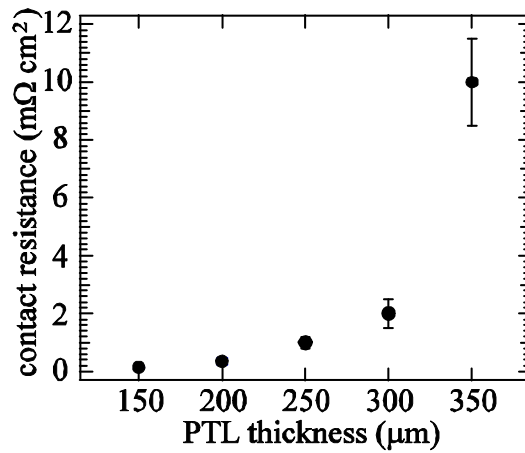


Figure 33. Contact resistance between PTL and graphite.

#### 5.4.2. Modeling

The experimentally evaluated parameter values were used in a computer model to see the effect of inhomogeneous compression of PTL on cell performance. After the Publications VI and VII were published and initial results presented, the following inaccuracies were found:

- In the liquid water saturation function, it was assumed that the density of liquid water and water vapor were the same.
- The molar fraction of water vapor at the boundary II should be 0.095 in stead of 0.077.
- The porosity of compressed PTL should be calculated with the function

$$\varepsilon(x) = 1 - (1 - \varepsilon_0) \frac{h_0}{h}$$

These uncertainties affect slightly the mass transfer in the cell. The model was amended, and the results reported here are calculated using the corrected model. However, the transport parameters of liquid water were not known, which limits the model to one-phase conditions and thus the first error does not affect the analysis of the results.

The calculated polarization curves are presented in Figure 34. The performance of the cell is slightly weaker when the inhomogeneous compression is taken into account. The difference is due to increased ohmic losses, caused by poor contact between the electrode and PTL under the channel. It must be noted that with the current choice of parameters, the cell has significantly high activation overpotential.

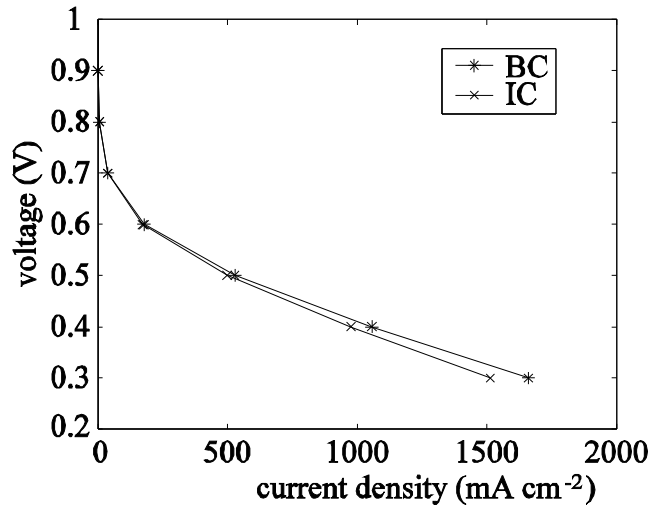


Figure 34. Modeled polarization curves with “base case” (BC) and “real case” (IC).

The molar fraction of water exceeded the saturation limit at approximately 0.49 V for both cases. Due to unknown two-phase parameters, this is the lower voltage limit for the validity of the model. The molar fraction of oxygen at the electrode-contact layer interface for both cases at 0.5 V is illustrated in Figure 35. There are no notable changes in the distribution of oxygen. The inhomogeneous compression does not affect the mass transfer significantly due to high porosity and permeability of tested PTL material.

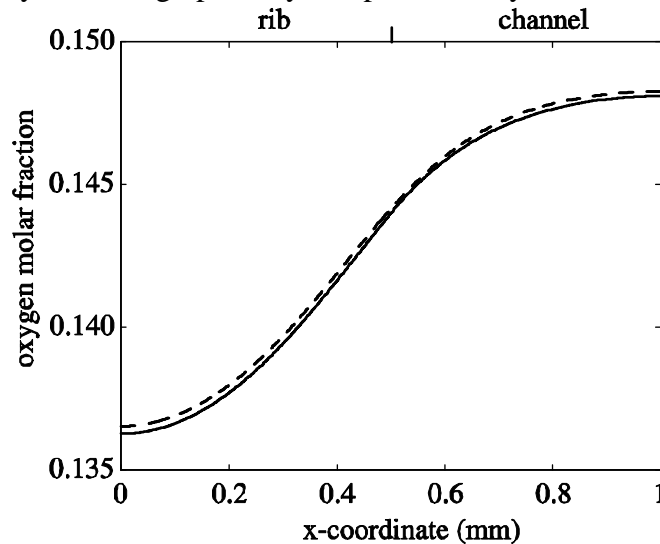


Figure 35. Molar fraction of oxygen at the electrode-contact layer interface at 0.5 V cell voltage. Dashed line: “base case”, solid line: “real case”.

The inhomogeneous compression of PTL has a significant effect on the local current distribution. Current distributions in the middle of the contact layer are shown in Figure 36. Current distribution with the base case is almost constant. When inhomogeneous compression is taken into account, there is a large peak in the middle of the modeled geometry, at the edge of the rib. This is due to large contact resistance between the electrode and PTL under the channel. A significant portion of the current produced under the channel flows along the electrode in lateral direction and enters the PTL where the contact resistance is smaller. Similar peak was observed also on the anode side.

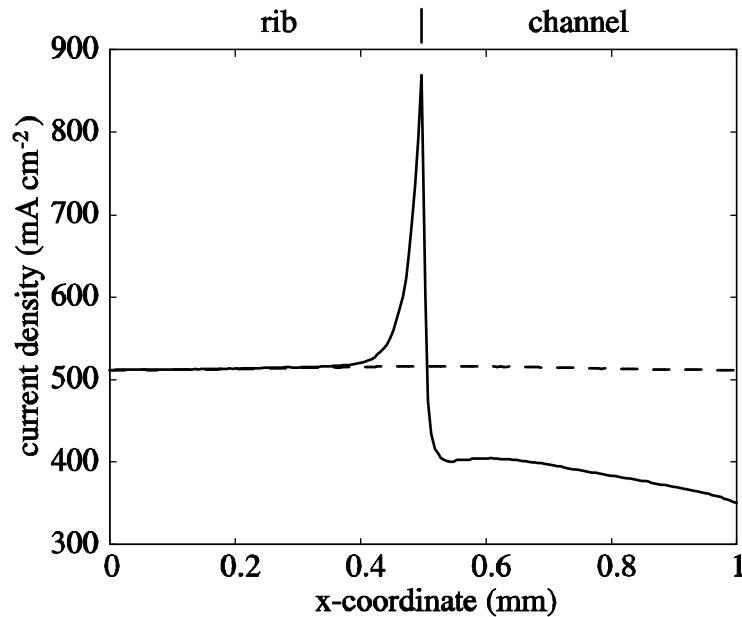


Figure 36. Current distributions in the middle of the cathode side contact layer at 0.5 V cell voltages. Dashed line: “base case”, solid line: “real case”.

Freunberger et al. [91] measured the current distribution from the cathode-PTL contact with sub-millimeter resolution. Their results show current peaking under the edge of the rib at current densities less than  $600 \text{ mA cm}^{-2}$ . With higher current densities, the oxygen transfer limitations moved the current peak under the channel. This movement of the current peak was not noticed in Publications VI and VII most probably due to smaller current densities and different PTL properties.

The inhomogeneous compression of PTL has also a significant effect on the temperature distribution in the cell. The modeled temperature distribution of the cell when inhomogeneous compression is taken into account is presented in Figure 37. A high thermal contact resistance between PTL and electrode under the channel causes a lateral heat flux towards to the areas where the contact resistance is smaller. Highest temperatures were at the cathode under the center of the channel. At 0.5 V, the temperature differences inside the cell are approximately  $13 \text{ }^\circ\text{C}$ . The temperature difference over the PTL-electrode contact varies from  $1 \text{ }^\circ\text{C}$  under to rib to  $9 \text{ }^\circ\text{C}$  under the channel. In the base case, the temperature difference inside the cell is significantly

smaller, 5 °C, and the temperature difference over PTL-electrode contact is approximately 1 °C.

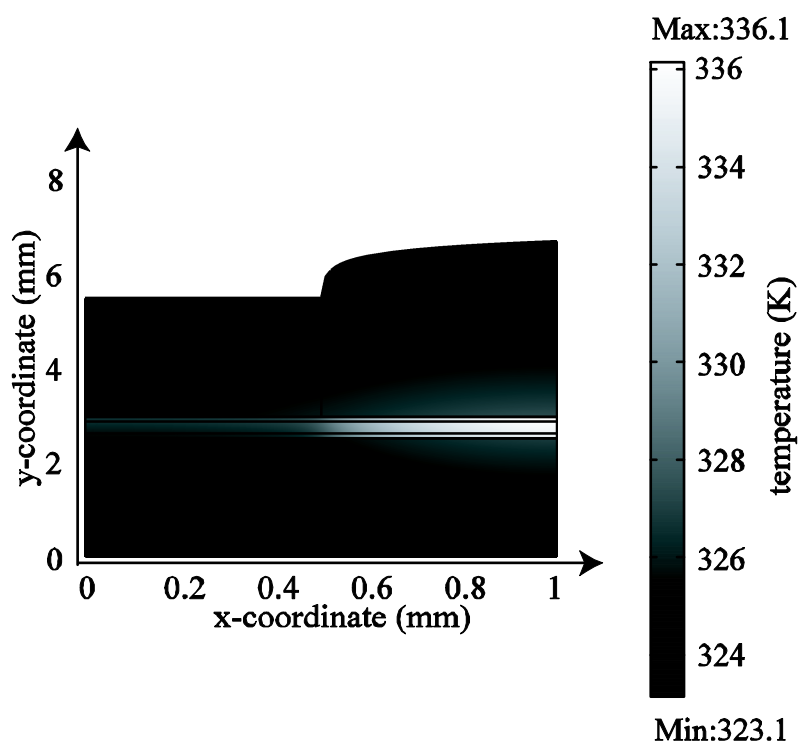


Figure 37. Modeled temperature distribution at 0.5 V cell voltage.

## 6. Summary and Conclusions

The aim of this thesis was to increase understanding of transport phenomena in small PEMFCs. In small PEMFC systems, passive controlling methods should be used to minimize power consumption of auxiliary components. Passive controlling methods are based on material and structural solutions, and knowledge of material parameters and transport phenomena is essential.

Water management is one of the most important issues for PEMFCs. A new method was developed and successfully demonstrated for the evaluation of water transport properties of MEA under real operating conditions. Measurements were carried out with a symmetrical H<sub>2</sub>-H<sub>2</sub> cell and combined with a computer model. Modeling was found necessary because of uneven water distribution inside the cell. The diffusion coefficient of water in the membrane of GORE™ Series 58 MEA was obtained. The developed method can be used to characterize MEAs under real operating conditions, which is important for the development of new MEAs and for the choice of suitable MEA for each application.

The operation of a free-breathing PEMFC was investigated at low temperatures. The cell was able to operate even at -27.5 °C if the current density and heat production of the cell were high enough. The cold start of the cell was found to be problematic under -5 °C, and at cold temperatures the cell needs active heating for reasonable start-up time. Irreversible performance losses will occur if the water freezes inside the cell and it must be avoided using insulation, heating, drying or anti-freeze chemicals. The operation of a free-breathing PEMFC in dead-end mode with high hydrogen utilization rate (0.95) was also demonstrated. The hydrogen outlet has to be equipped with a purge valve, which enables periodical flushing of the anode to remove excess water and inert gases. The purge valve is also important for the start-up of the cell, especially after a long non-operating period, because air may replace hydrogen in the anode compartment. Functionality of water management and mass transport of free-breathing PEMFC in a dead-end mode and at low temperature were successfully demonstrated, which are important for their use in real applications.

When a PEMFC is assembled, the porous transport layers are compressed inhomogeneously, which affects the transport phenomena inside the cell. Experiments showed that the PTL in the middle of the channel remains almost uncompressed, and gas permeability and electrical parameters depend strongly on the compressed thickness of PTL. Modeling work showed that inhomogeneous compression does not significantly affect cell polarization behavior or mass transfer, but has a huge effect on current and temperature distributions. Due to large contact resistance between the electrode and porous transport layer, the current and heat produced under the channel flow along the electrode and enter the PTL where the contact resistance is smaller. This creates a current peak at the edge of the rib and high temperature differences into the cell. Current density and temperature distributions should be as even as possible to maximize cell performance and lifetime. Therefore, the areas having high contact resistance on both sides should be minimized by flow field design. This can be done e.g. with a cross-flow mode. Inhomogeneous compression of PTL has significant effects on PEMFC operation and must be taken into account when designing or modeling PEMFCs.

In the future, water transport by hydraulic permeation and electro-osmotic drag should be studied using a similar approach as with diffusive water transport measurements presented here. Water transport and water uptake measurements should be carried out with an MEA and also with a plain membrane to separate their effects. This would provide a good technique for the characterization of their water transport properties. More parameters related to deformation of PTL, like thermal properties, geometry of PTL in the channel, and contact resistance between electrode, should be evaluated. These parameters could be combined with water transport studies to obtain a good model based on experimental results to support PEMFC development. This would be very useful in the design of PEMFCs and their controlling systems and procedures. Two-phase effects should be studied to get reliable parameter values for the modeling. A free-breathing PEMFC should be combined with small hydrogen generator and the operation of the system investigated in a dead-end mode and also at low temperatures. Especially freeze prevention and cold start methods of the system should be developed to enable rapid start-up essential for real applications.

## References

- [1] F. Barbir, PEM Fuel Cells: Theory and Practice, Elsevier Academic Press, 2005, USA, ISBN 0-12-078142-5
- [2] M. Wilson, J. Valerio, S. Gottesfeld, *Electrochimica Acta* 40(3), pp. 355-363, 1995
- [3] H. Zhong, H. Zhang, G. Liu, Y. Liang, J. Hu, B. Yi, *Electrochem. Commun.* 8, pp. 707-712, 2006
- [4] X. Yu, S. Ye, *J. Power Sources* 172, pp. 145-154, 2007
- [5] J. Kolde, B. Bahar, M. Wilson, T. Zawodzinski, S. Gottesfeld, *Advanced Composite Polymer Electrolyte Fuel Cell Membranes, Proc. Of the First International Symposium on Proton Conducting Membrane Fuel Cells I Electrochemical Society Proceedings, Vol. 95-23*, pp. 193-201, 1995
- [6] B. Pivovar, W. Smyrl, E. Cussler, *J. Electrochem. Soc.* 152(1), pp. A53-A60, 2005
- [7] K. Kreuer, *Chem. Mater.* 8, pp. 610-641, 1996
- [8] S. Cleghorn, J. Kolde, W. Liu, in *Handbook of Fuel Cells*, Eds. W. Vielstich, A. Lamm, H. Gasteiger, John Wiley & Sons, Ltd., UK, 2003, ISBN 0-471-49926-9
- [9] P. Rieke, N. Vanderborgh, *J. Membr. Sci.* 32(2-3), pp. 313-328, 1987
- [10] T. Zawodzinski, M. Neeman, L. Sillerud, S. Gottesfeld, *J. Phys. Chem.* 95, pp. 6040-6044, 1991
- [11] J. Gostick, M. Fowler, M. Ioannidis, M. Pritzker, Y. Volfkovich, A. Sakars, *J. Power Sources* 156, pp. 375-387, 2006
- [12] B. Peppley, H. Atiyeh, E. Halliop, K. Karan, J. Pharoah, A. Phoenix, in *WHEC 16*, 13-16.6.2007, Lyon, France
- [13] S. Karvonen, T. Hottinen, J. Saarinen, O. Himanen, *J. Power Sources* 161, pp. 876-884, 2006
- [14] F. Barreras, A. Lozano, L. Valiño, C. Marin, A. Pascau, *J. Power Sources* 144, pp. 54-66, 2005
- [15] Y. Ferng, A. Su, S. Lu, *Int. J. Energy Res.*, DOI: 10.1002/er.1320, in Press, 2007
- [16] J. Evertz, M. Günthart, in: *Proceedings of 2<sup>nd</sup> European PRFC Forum, Vol. 2*, pp. 469-482, Lucerne, Switzerland, 2003
- [17] S. Lee, C. Hsu, C. Huang, *J. Power Sources* 145, pp. 353-361, 2005

- [18] M. Noponen, T. Mennola, M. Mikkola, T. Hottinen, P. Lund, *J. Power Sources* 106, pp. 304-312, 2002
- [19] M. Noponen, T. Hottinen, T. Mennola, M. Mikkola, P. Lund, *J. Appl. Electrochem.* 32, pp. 1081-1089, 2002
- [20] T. Hottinen, M. Noponen, T. Mennola, O. Himanen, M. Mikkola, P. Lund, *J. Appl. Electrochem.* 33, pp. 265-271, 2003
- [21] T. Mennola, M. Noponen, M. Aronniemi, T. Hottinen, M. Mikkola, O. Himanen, P. Lund, *J. Appl. Electrochem.* 33, pp. 979-987, 2003
- [22] T. Hottinen, M. Mikkola, P. Lund, *J. Power Sources* 129, pp. 68-72, 2004
- [23] T. Hottinen, O. Himanen, P. Lund, *J. Power Sources* 138, pp. 205-210, 2004
- [24] S. Jeong, E. Cho, H. Kim, T. Lim, I. Oh, S. Kim, *J. Power Sources* 158, pp. 348-353, 2006
- [25] A. Schmitz, S. Wagner, R. Hahn, H. Uzun, C. Hebling, *J. Power Sources* 127, pp. 197-205, 2004
- [26] A. Schmitz, M. Tranitz, S. Eccarius, A. Weil, C. Hebling, *J. Power Sources* 154, pp. 437-447, 2006
- [27] R. Hahn, S. Wagner, A. Schmitz, R. Reichl, *J. Power Sources* 131, pp.73-78, 2004
- [28] Y. Tabe, S. Park, K. Kikuta, T. Chikahisa, Y. Hishinuma, *J. Power Sources* 162, pp. 58-65, 2006
- [29] T. Hottinen, O. Himanen, P. Lund, K. Åström, High Power Density Thin PEMFC for Portable Applications, Poster Presentation in 2004 Fuel Cell Seminar, 1.-5.11.2004, San Antonio, Texas, USA
- [30] J. Zhang, Y. Tang, C. Song, J. Zhang, H. Wang, *J. Power Sources* 163, pp. 532-537, 2006
- [31] A. Bard, L. Faulkner, *ELECTROCHEMICAL METHODS Fundamentals and Applications* 2<sup>nd</sup> Edition, John Wiley & Sons, Inc., USA, 2001, ISBN 0-471-04372-9
- [32] K. Lum, J. McGuirk, *J. Electrochem. Soc.* 152(4), pp. A811-A817, 2005
- [33] M. Serincan, S. Yesilyurt, *Fuel Cells* 7(2), pp. 118-127, 2007
- [34] T. Zawodzinski, C. Derouin, S. Radzinski, R. Sherman, V. Smith, T. Springer, S. Gottesfeld, *J. Electrochem. Soc.* 140(4), pp. 1041-1047, 1993

- [35] M. Mathias, J. Roth, J. Fleming, W. Lehnert, in Handbook of Fuel Cells, Eds. W. Vielstich, A. Lamm, H. Gasteiger, John Wiley & Sons, UK, 2003, ISBN 0-471-49926-9
- [36] T. Springer, M. Wilson, S. Gottesfeld, J. Electrochem. Soc. 140(12), pp. 3513-3526, 1993
- [37] T. Springer, T. Zawodzinski, M. Wilson, S. Gottesfeld, J. Electrochem. Soc. 143(2), pp. 587-599, 1996
- [38] J. Itonen, M. Mikkola, G. Lindbergh, J. Electrochem. Soc. 151(8), pp. A1152-A1161, 2004
- [39] E. Birgersson, M. Vynnycky, J. Power Sources 153, pp. 76-88, 2006
- [40] W. Yan, C. Yang, C. Soong, F. Chen, S. Mei, J. Power Sources 160, pp. 284-292, 2006
- [41] T. Springer, T. Zawodzinski, S. Gottesfeld, J. Electrochem. Soc. 138(8), pp. 2334-2342, 1991
- [42] H. Ju, C. Wang, S. Cleghorn, U. Beuscher, J. Electrochem. Soc. 152(8), pp. A1645-A1653, 2005
- [43] P. Nguyen, T. Berning, N. Djijali, J. Power Sources 130, pp. 149-157, 2004
- [44] U. Pasaogullari, C. Wang, J. Electrochem. Soc. 152(2), pp. A380-A390, 2005
- [45] C. Ziegler, A. Schmitz, M. Tranitz, E. Fontes, J. Schumacher, J. Electrochem. Soc., 151(12), pp. A2028-A2041, 2004
- [46] A. Weber, J. Newman, J. Electrochem. Soc. 151(2), pp. A311-A325, 2004
- [47] K. Dannenberg, Ph.D Thesis, Royal Institute of Technology, Stockholm, Sweden, 2002
- [48] Q. Yan, H. Toghiani, J. Wu, J. Power Sources 158, pp. 316-325, 2006
- [49] T. Zawodzinski, J. Davey, J. Valerio, S. Gottesfeld, Electrochim. Acta 40(3), pp. 297-302, 1995
- [50] F. Meier, G. Eigenberger, Electrochim. Acta 49, pp. 1731-1742, 2004
- [51] J. Cao, N. Djijali, J. Energy Resources Tech. 127, pp. 26-36, 2005
- [52] T. Fuller, Ph.D. Thesis, University of California, Berkeley, USA, 1992
- [53] S. Motupally, A. Becker, J. Weidner, J. Electrochem. Soc. 147(9), pp. 3171-3177, 2000

- [54] S. Ge, X. Li, B. Yi, I. Hsing, J. Electrochem. Soc. 152(6), pp. A1149-A1157, 2005
- [55] X. Ye, M. LeVan, J. Membr. Science 221, pp. 147-161, 2003
- [56] I. Nicotera, T. Zhang, A. Bocarsly, S. Greenbaum, J. Electrochem. Soc. 154(5), pp. B466-B473, 2007
- [57] X. Gong, A. Bandis, A. Tao, G. Meresi, Y. Wang, P. Inglefield, A. Jones, W. Wen, Polymer 42, pp. 6485-6492, 2001
- [58] S. Yeo, A. Eisenberg, J. Appl. Polym. Sci. 21, pp. 875-898, 1977
- [59] F. Damay, L. Klein, Solid State Ionics 162-163, pp. 261-267, 2003
- [60] H. Yeager, A. Steck, J. Electrochem. Soc. 128, pp. 1880-1884, 1981
- [61] G. Suresh, Y. Scindia, A. Pandey, A. Goswami, J. Membrane Science 250, pp. 39-45, 2005
- [62] T. Mennola, M. Mikkola, M. Noponen, T. Hottinen, P. Lund, J. Power Sources 112, pp. 261-272, 2002
- [63] W. Wruck, R. Machado, T. Chapman, J. Electrochem. Soc. 134(3), pp. 539-546, 1987
- [64] C. Lagergren, G. Lindbergh, D. Simonsson, J. Electrochem. Soc. 142(3), pp. 787-797, 1995
- [65] B. Andreaus, A. McEvoy, G. Scherer, Electrochim. Acta, 47, pp. 2223-2229, 2002
- [66] M. Ciureanu, H. Wang, J. Electrochem. Soc. 146(11), pp. 4031-4040, 1999
- [67] Y. Tang, J. Zhang, C. Song, H. Liu, J. Zhang, H. Wang, S. Mackinnon, T. Peckham, J. Li, X. McDermid, P. Kozak, J. Electrochem. Soc. 153(11), pp. A2036-A2043, 2006
- [68] F. Richter, C. Schiller, N. Wagner, Electrochemical Applications, 1/2002, ZAHNER-elektrik GmbH, 2002
- [69] J. Itonen, F. Jaouen, G. Lindbergh, G. Sundholm, Electrochim. Acta 46, pp. 2899-2911, 2001
- [70] E. Barsoukov, J. Macdonald, Impedance Spectroscopy, John Wiley & Sons, Inc., USA, 2005, ISBN 0-471-64749-7
- [71] T. Pajkossy, Solid State Ionics 176, pp. 1997-2003, 2005

- [72] K. Wiezell, P. Gode, G. Lindbergh, *J. Electrochem. Soc.* 153(4), pp. A759-A764, 2006
- [73] J. Hinatsu, M. Mizuhata, H. Takenaka, *J. Electrochem. Soc.* 141(6), pp. 1493-1498, 1994
- [74] T. Nguyen, R. White, *J. Electrochem. Soc.* 140(8), pp. 2178-2186, 1993
- [75] E. Cho, J. Ko, H. Ha, S. Hong, K. Lee, T. Lim, I. Oh, *J. Electrochem. Soc.* 150(12), pp. A1667-A1670, 2003
- [76] E. Cho, J. Ko, H. Ha, S. Hong, K. Lee, T. Lim, I. Oh, *J. Electrochem. Soc.* 151(5), pp. A661-A665, 2004
- [77] J. Hou, H. Yu, S. Zhang, S. Sun, H. Wang, B. Yi, P. Ming, *J. Power Sources* 162, pp. 513-520, 2006
- [78] K. Tajiri, Y. Tabuchi, C. Wang, *J. Electrochem. Soc.* 154(2), pp. B147-B152, 2007
- [79] L. Mao, C. Wang, *J. Electrochem. Soc.* 154(2), pp. B139-B146, 2007
- [80] M. Oszcipok, D. Riemann, U. Kronenwett, M. Kreideweis, M. Zedda, *J. Power Sources* 145, pp. 407-415, 2005
- [81] M. Oszcipok, M. Zedda, D. Riemann, D. Geckeler, *J. Power Sources* 154, pp. 404-411, 2006
- [82] M. Sundaresan, R. Moore, *Fuel Cells* 4, pp. 476-485, 2005
- [83] M. Sundaresan, R. Moore, *J. Power Sources* 145, pp. 534-545, 2005
- [84] Q. Yan, H. Toghiani, Y. Lee, K. Liang, H. Causey, *J. Power Sources* 160, pp. 1242-1250, 2006
- [85] S. Chan, Z. Xia, Z. Wei, *J. Power Sources* 158, pp. 385-391, 2006
- [86] W. Zhu, R. Payne, B. Tatarchuk, *J. Power Sources* 156, pp. 512-519, 2006
- [87] D. McKay, W. Ott, A. Stefanopoulou, in: *Proceedings of IMECE'05 2005 ASME International Mechanical Engineering Congress & Expedition, Orlando, USA, 5-11 November, 2005*
- [88] E. Carlson, P. Kopf, J. Sinha, S. Sriramulu, Y. Yang, NREL Subcontract Report NREL/SR-560-39104, <http://www.nrel.gov/hydrogen/pdfs/39104.pdf>, 2005
- [89] W. Sun, B. Peppley, K. Karan, *J. Power Sources* 144 pp. 42-53, 2005
- [90] P. Zhou, C. Wu, J. Ma, *J. Power Sources* 159, pp. 1115-1122, 2006

- [91] S. Freunberger, M. Reum, J. Evertz, A. Wokaun, F. Büchi, J. Electrochem. Soc. 153(11), pp. A2158-A2165, 2006
- [92] [http://sglcarbon.de/sgl\\_t/fuelcell/index.html](http://sglcarbon.de/sgl_t/fuelcell/index.html), datasheet of SGL Series 10 GDL, cited 15.3.2007
- [93] M. Yamaguchi, N. Matsuo, S. Uozumi, Japanese Patent H6-84529
- [94] K. Kodama, Japanese Patent P2004-178893A
- [95] A. Caillard, P. Brault, J. Mathias, C. Charles, R. Boswell, T. Sauvage, Surf. Coatings Technol. 200, pp. 391-394, 2005
- [96] I. Nitta, O. Himanen, manuscript to be submitted, 2007
- [97] J. Gostick, M. Fowler, M. Pritzker, M. Ionnidis, L. Behra, J. Power Sources 162, pp. 228-238, 2006
- [98] M. Williams, E. Begg, L. Bonville, H. Kunz, J. Fenton, J. Electrochem. Soc. 151(8), pp. A1173-A1180, 2004
- [99] M. Mench, C. Wang, J. Electrochem. Soc. 150(1), pp. A79-A85, 2003
- [100] D. Natarajan, T. Nguyen, J. Power Sources 135, pp. 95-109, 2004
- [101] S. Nakamura, T. Tomimura, H. Nonami, H. Saito, Proc. of the IEEE 7<sup>th</sup> International Conference on Solid Dielectrics, pp.101-104, 2001
- [102] V. Mishra, F. Yang, R. Pitchumani, J. Fuel Cell Sci. Technol. 1, pp. 2-9, 2004



ISBN 978-951-22-9146-5  
ISBN 978-951-22-9147-2 (PDF)  
ISSN 1795-2239  
ISSN 1795-4584 (PDF)